This is the peer-reviewed, final accepted version for American Mineralogist, published by the Mineralogical Society of America.
The published version is subject to change. Cite as Authors (Year) Title. American Mineralogist, in press.
DOI: https://doi.org/10.2138/am-2022-8728. http://www.minsocam.org/

Revision 2

A possible origin of the lunar spinel-bearing lithologies as told by the meteorite NWA 13191

LAN F. XIE[1], HONG Y. CHEN[1,*], BING K. MIAO[1,*], WEN L. SONG[2],
ZHI P. XIA[1], GUO Z. CHEN[1], JIN Y. ZHANG[1], SI Z. ZHAO[1, 3], XU K. GAO[1]

[1] Key Laboratory of Planetary Geological Evolution of Guangxi Provincial Universities and Guangxi Key Laboratory of Hidden Metallic Ore Deposits Exploration, College of Earth Sciences, Guilin University of Technology, Guilin 541006, China
[2] State Key Laboratory of Continental Dynamics, Department of Geology, Northwest University, Xi'an 710069, China.
[3] Center for Lunar and Planetary Sciences, Institute of Geochemistry, Chinese Academy of Sciences, Guiyang 550081, China

ABSTRACT

Pink spinel anorthosite (PSA) and pink spinel troctolite (PST) are two lunar lithologies known to contain Mg-rich spinel. PSA rich in spinel and lacking mafic minerals, was detected by the visible and near-infrared reflectance spectroscopy. PST clasts were found in returned lunar samples and meteorites. NWA 13191 is a recently approved lunar meteorite that contains a large amount of spinel-bearing clasts and provides an opportunity to discuss its origin. In this paper, 64 spinel-bearing clasts are studied. These clasts are dominated by anorthitic feldspars (20.8 – 80.9 vol.%, $An_{90.9-96.8}$), mafic-rich and aluminum-rich melt (14.7 – 72.1 vol.%) and spinels (0.19 – 5.18 vol.%). 49 of these clasts appears to have an unusually low modal abundance of mafic silicates (avg. olivine ± pyroxene, 1.87 vol.%), which distinguishes it from known spinel-bearing lunar samples (e.g., PST). The spinel composition (avg. $Mg^{\#}$ = 90.6, $Al^{\#}$ = 97.4) and mafic minerals content are basically consistent with those of PSA. The absorption characteristics of the melt in the reflection spectrum are not obvious, so it is not clear if the PSA contains melt. The simulated crystallization experiment clearly shows that it contains a large amount of melt at the spinel crystallization stage. These phenomena provide experimental and sample evidences for the existence of melt in the lunar spinel-bearing lithologies. NWA 13191 records the highest known bulk $Mg^{\#}$ (avg. 89.8) and the spinel records the highest $Al^{\#}$ (98.8) and $Mg^{\#}$ (93.1) of lunar samples to date. The chemical properties of spinel-bearing clasts in NWA 13191 are consistent with the slightly REE-enriched and alkali-poor Mg-suite rocks, such as PST, magnesian anorthosites (MANs), and olivine-enriched Mg-suite rocks. These phenomena and previous simulated crystallization experiments indicate that the Mg-Al-rich melt may be produced by impact melting of Mg-rich anorthosite precursors. The spinel is a metastable crystallization product along with plagioclase and vitric melt near the Moon's surface. This realization provides sample observational evidence for previous simulated crystallization experiments and theoretical speculations.

Key words: Lunar meteorite, spinel, Mg-rich anorthosites, origin, impact melting, PSA, PST

INTRODUCTION

PSA has been identified and defined by high-resolution mineralogical data (Pieters et al., 2011) from NASA's test load Moon Mineralogy Mapper (M^3) aboard the Chandrayaan-1 spacecraft (Pieters et al., 2009). The term PSA was adopted in homage to PST lithics of lunar Mg-suite samples (e.g., Prinz et al., 1973; Marvin et al., 1989). PSA shows no detectable absorption feature near 1000 nm, but it has a prominent absorption centered near 2000 nm (Pieters et al., 2010; 2011; Taylor and Pieters et al., 2013), thus PSA contains nearly pure $MgAl_2O_4$ spinel (hereafter referred as spinel), and unusually low abundances of mafic minerals. The abundances of olivine ± pyroxene are estimated to be no more than 5 vol.% for the PSA lithology, based on laboratory spectra and nonlinear mixing calculations (e.g., Dhingra et al., 2011; Cheek and Pieters, 2014). Lunar troctolitic cataclasites contain few spinel, only two contain more than ~ 5 – 6 vol.% spinel (Gross et al., 2014 and references therein), but these PSA outcrop zones are inferred to contain 20 – 30% spinel (Taylor and Pieters, 2013). Crystallization experiments on the composition of AHLA 81005 PST fragment (350 × 150 μm, ~ 30 vol.% spinel, Gross et al., 2011; Gross and Treiman,

Always consult and cite the final, published document. See http:/www.minsocam.org or GeoscienceWorld

2011) did not yield spinel; however, compositon similar to Apollo 65785 (~ 13 vol.% spinel, Prinz et al., 1973) crystallized ~ 8 vol.% spinel. Thus, the spinel-rich outcrop zones might not be as spinel-rich as previously thought and may only represent ~ 4 – 5 wt.% spinel (Gross et al., 2014). Sun et al. (2016) applied the spinel-pyroxene mixture model to the spectra detected by M^3 data for Tycho Crater and showed that the spinel represents only 5.4 – 6.4 vol.% of the spinel-pyroxene mix. However, only need 5 vol.% spinel ($Mg^{\#}$ = 87) in the mixture samples to mask the crystalline plagioclase band and generate the 2000 nm absorption (Cheek et al., 2014). The PSA spectral data are consistent with spinels having $Mg^{\#}$ ＞ 88 (100 × Mg / [Mg + Fe], molar) (Jackson et al., 2014) and potentially $Al^{\#}$ ＞ 99 (100 × Al / [Cr + Al], molar) (Williams et al., 2016) , based on the compositional and spectral analyses of synthesized spinel. The spinel is typically found in a dominantly anorthositic terrain, so the remaining mineral is inferred to be plagioclase (Dhingra et al., 2011), but its content is still relatively unconstrained. No plagioclase absorption (~ 1250 nm) is observed in these remote data, which could be due either to the effects of shock metamorphism destroying the plagioclase crystal structure or spinel masking the absorption of plagioclase crystal (Cheek et al., 2014). With the above comprehensive analysis, the main characteristics of PSA can be modified from Taylor and Pieters (2013): consist of ~ 5 – 8 vol.% spinel, base on mixture spectral experiments; with < 5 vol.% mafic mineral， and ＞ 90 vol.% crystallized or shocked plagioclase; have < 10 wt.% FeO (Pieters et al., 2011) and high-$Mg^{\#}$, low-FeO melt. The exact chemical or physical property of the lithology remains in question due to lack of laboratory samples.

Possible explanations for the petrogenesis of spinel-bearing lithologies range from low-pressure near-surface crystallization to a deep source in the lower lunar crust or upper mantle (Gross et al., 2014 and references therein). Three major hypotheses have been put forward: a. spinel formed at low pressure by impact melting of Mg-rich anorthosite precursors, such as troctolite or troctolitic anorthosite (Treiman et al., 2010). Low-pressure experiments on Apollo samples indicate that olivine + plagioclase components could be produced by partial or complete melting of Mg-rich anorthosites or troctolite materials from the lunar crust, and not necessarily by partial melting of material from the deep Moon (Walker et al., 1973). This hypothesis was confirmed by low-pressure experiments on plagioclase-olivine melt from natural samples (Marvin and Walker, 1985). b. Spinel formed at low pressure by chemical reaction between picritic magma or Mg-suite parental melts and anorthositic crust (Morgan et al., 2006; Gross and Treiman, 2011; Prissel et al., 2014). c. Spinel formed at high pressure in the deep crust (≥ ~ 25 – 60 km), from basaltic or peridotitic precursors (Herzberg and Baker, 1980; Marvin et al., 1989; Wittmann et al., 2019). The hypotheses b and c contradict the apparent lack of mafic minerals in the PSA, because the picritic, basaltic, and peridotitic magma can produce abundant mafic minerals. This key phenomenon can be explained if the precursor material of olivine + plagioclase components undergoes shock melting and then recrystallizes at low pressure and high temperature to form spinel. Crystallization experiments at 1 bar (this pressure would be produced during cooling of a large impact melt sheet) conducted on olivine and plagioclase-rich rock compositions (e.g., Apollo PST 65785) show that the crystallized product is spinel ($Mg^{\#}$ = 93.9 – 90.5, 3.0 – 8.0 wt.%) + plagioclase (≤ 39.6 wt.%) + glass (97.0 – 50.9 wt.%) + olivine (≤ 1.2 wt.%) at 1450 °C – 1300 °C; olivine appears abundantly (~ 13.6 wt.%) , while spinel (5.2 wt.%, $Mg^{\#}$ = 88.6) is relatively iron-rich at 1250 °C (Gross et al., 2014).

PSA is distributed on both the near and far side of the Moon. It was found in central peaks of 23% of the craters studied by Sun et al. (2017). This indicates that the formation of PSA may have occurred on a global scale. PST clasts found in Lunar samples (e.g., Prinz et al., 1973; Herzberg and Baker, 1980; Marvin et al., 1989; Cohen et al., 2001) and lunar meteorites (e.g., Gross and Treiman, 2011; Wittmann et al., 2019) are the closest samples to the spectroscopic interpretation of the spinel composition. However, the spinel is general slightly richer in Fe and Cr than that in PSA, just one clastic particle from the regolith breccia 10019 (Keil et al., 1970) and spinel-bearing troctolite 2003 from Luna 20 (Cohen et al., 2001) are the only two samples with small amounts of near-pure spinel ($Mg^{\#}$ ~ 93, $Al^{\#}$ ~ 98; $Mg^{\#}$ ~ 91, $Al^{\#}$ ~ 98, respectively) matching PSA. However, every known spinel-bearing lunar

Always consult and cite the final, published document. See http:/www.minsocam.org or GeoscienceWorld

DOI: https://doi.org/10.2138/am-2022-8728. http://www.minsocam.org/

sample contains significant proportions of olivine ± pyroxene (＞8 vol.%), which is inconsistent with an approximately mafic-free PSA lithology.

PSA is a MgO-rich, FeO-poor anorthosite. However, due to the lack of relevant samples, for the component and formation of the PSA, there is no direct evidence for its petrology, mineralogy, and major and trace element geochemistry. This paper presents a recently discovered lunar meteorite, spinel-bearing polymict breccia NWA 13191. Sixty-four typical spinel-bearing clasts are selected as the main objects of study. Through systematic petrological, mineralogical and geochemical studies, we aim to compare the sample with known PST clasts with similar chemical characteristics, and investigate its relationship to the PSA. In addition, analysis of the origin and chemical properties of the melt, spinel and olivine, elucidates the formation of spinel-bearing clasts in the NWA 13191 meteorite.

SAMPLE AND ANALYTICAL METHODS

Sample preparation

NWA 13191 is a spinel-bearing feldspathic breccia of lunar provenance, as will be shown later in the paper. The size of the hand specimen is ca. 9 × 4 × 3 cm. The fusion crust is missing, while the stone is covered with yellow-brown desert varnish (Fig. 1). In this paper, a 4.5 × 2.5 cm thin section of NWA 13191, 2 is used for petrological observation and analysis of the chemical composition of minerals (Fig. 2). A total of 130 mg of sub-samples are collected from the powder in the diamond wire saw cutting process and some fragments (particle size ~ 1 mm) in five different areas from the rim to core of the thin section. These fragments and powders can represent the average composition of the whole rock. The fragments are ground to less than 20 μm with an agate mortar. Therein samples of 30 mg are analyzed by the New Microprobe Fused Bead (NMFB) method for bulk major elements, and samples of 100 mg are measured by Inductively Coupled Plasma Mass Spectrometry (ICP–MS) for bulk trace elements.

Instruments and analytical methods

Scanning Electron Microscopy (SEM), Electron Probe Microanalyzer (EPMA), Laser Ablation Inductively Coupled Plasma Mass Spectrometry (LA–ICP–MS) and ICP–MS analytical data are obtained at the Guangxi Key Laboratory of Hidden Metallic Ore Deposits Exploration, Guilin University of Technology (GUT). Backscattered electron (BSE) images of carbon-coated polished thin section are obtained using a ∑IGMA field emission SEM. An electron beam with an accelerating voltage of 15 kV and a 20 nA current is used. Major element compositions of spinel, plagioclase, olivine, pyroxene and glass are determined using a JEOL JXA-8230 EPMA. Spot analyses are performed on all minerals and glass using an electron beam with an accelerating voltage of 15 kV. The plagioclase are analyzed using a 5 μm diameter electron beam and a current of 10 nA. Spinel, glass, olivine and pyroxene are analyzed using a focused electron beam (＜1 μm) and a current of 20 nA. Natural and synthetic crystals are used as standards for the analyses ZAF correction was applied to all analyses. The standard materials used for the calibration of measured elements and their limit of detection (ppm) were: Si (olivine, 130); Ti (rutile, 294); Al (albite, 88); Cr (Cr metal, 83); Fe (olivine, 154); Mn (MnO, 104); Mg (olivine, 130); Ca (wollastonite, 91); Na (albite, 97); K (phlogopite, 77); Ni (Ni metal, 201).

The X-ray mapping (Fig. 2) and the modes of the minerals (vol.%) are obtained using a TESCAN Integrated Mineral Analyzer (TIMA) system at the State Key Laboratory of Continental Dynamics, Northwest University, Xi'an, China. TIMA is a SEM and energy disperse spectroscopy (SEM-EDS) based automated mineralogy system, comprising a TESCAN MIRA-3 SEM equipped with four EDS detectors, as well as mineral data processing software. TIMA is designed to automatically identify and quantify minerals based on the BSE signal intensity and characteristic X-rays spectrum. During analysis, the dot mapping analysis mode is choosen with X-ray counts set to 10000, pixel spacing of BSE set to 1.5 μm, and dot spacing of EDS set to 4.5 μm. The measurements are conducted at an acceleration voltage of 25 kV, current of 9 nA, and a working distance of 15 mm. The beam current and BSE signals are calibrated by platinum Faraday cup and EDS signals by Mn standard (Hrstka et al., 2018).

Always consult and cite the final, published document. See http:/www.minsocam.org or GeoscienceWorld

This is the peer-reviewed, final accepted version for American Mineralogist, published by the Mineralogical Society of America.
The published version is subject to change. Cite as Authors (Year) Title. American Mineralogist, in press.
DOI: https://doi.org/10.2138/am-2022-8728. http://www.minsocam.org/

The sample fabrication of NMFB method is performed at the Center for Lunar and Planetary Sciences, Institute of Geochemistry, Chinese Academy of Sciences. This method is an improvement on the Microprobe Fused Bead (MFB; for further information, see Brown, 1977) commonly used in Apollo samples, and solves the problems of volatilization of low-boiling elements and rapid crystallization of high-melting point minerals such as spinel and forsterite (Zeng et al., 2015). The main procedures are : (1) weigh 30 mg of the ground powder sample, put it into a pre-customized platinum tube, and seal the platinum tube port with a platinum cap (to prevent the escape of volatile elements); (2) a silicon-molybdenum rod lifting electric furnace is used to heat the packaged platinum tube, the whole heating process adopts nitrogen atmosphere, pressure 5 kPa, heating gradient: 20 – 500°C, 60 min; 500 – 800°C, 60 min; 800 – 1200 °C, 60 min; 1200 – 1480°C, 60 min; 1480°C, constant temperature for 120 min; (3) take out the sample and put it into cold water quickly, the whole quenching process is completed in 10 sec; (4) return the quenched sample into the electric furnace, and repeat the operation according to the above procedure to ensure the uniformity of the sintered glass sample; (5) the prepared glass sample and the platinum tube are processed into a polished thin section together. The bulk major elements of polished thin section are analyzed by EPMA at GUT.

Mineral phase is determined using a Renishaw inVia Raman spectrometer at the Key Laboratory of Nonferrous Metal Materials Processing Technology, Education Ministry of China, GUT, with a 20 mW, 780 nm Ar^+ laser (Feng et al., 2011). All tests are performed under a 100× objective lens with a laser focus of less than 1 μm. The spectral resolution is 1 cm^{-1}, and the Raman shift test range is 100 to 1300 cm^{-1}. Raman calibration is performed using monocrystal silicon wafers, where the Raman shift is 520.7 cm^{-1} .

Whole rock trace element analysis is carried out on an Agilent 7700 cx ICP–MS using a chemical dissolving method. *In situ* trace element analysis of minerals and melts is carried out by LA–ICP–MS. Operating conditions of the LA–ICP–MS instrument as well as data reduction are the same as described by Zong et al. (2017). Raw count rate data, including uncertainty, concentration and detection limit were reduced using the ICPMSDataCal software (Liu et al., 2008).

EXPERIMENTAL OBSERVATION AND ANALYTICAL RESULTS

Petrologic characteristics

NWA 13191 is an impact-melted polymict breccia (Fig. 1). Clast types include lithic clasts, glass and mineral fragments. Lithic clast mainly includes spinel-bearing lithologies, MANs, ferroan anorthosites (FANs), troctolite and fine-grained basalt. The glass fragments can be divided into mafic-rich, Al-rich, mixed and special components. The mafic-rich, Al-rich and mixed glass are related to spinel and can be collectively referred to as spinel-bearing vitric melt (hereafter referred to as melt). The mineral content of the whole rock is obtained using a TIMA instrument, namely plagioclase ± maskelynite (73.8 vol.%), pyroxene (13.4 vol.%), olivine (3.31 vol.%), spinel-bearing melt (7.95 vol.%), glass with special components (0.4 vol.%) and silica phase (0.28 vol.%). Other minerals are less than 0.1 vol.%, e.g., spinel, ilmenite, troilite, chromite, iron-nickel and terrestrial weathering materials (e.g., baryte and calcite) (Fig. 2).

Characteristics of major lithic clast

Spinel-bearing clasts are composed of plagioclase, mafic-rich and Al-rich melt, crystallized spinel, pyroxene, olivine-melt, as well as a small amount of silica phase, ilmenite, chromite, troilite, and iron-nickel, taking the distribution zone of spinel-bearing melt as the boundary of the spinel-bearing lithologies. The abundance of spinel-bearing clasts is ~8 vol.% according to the evaluation of Mg-Al-rich melt (Fig. 2). The size of the clasts is 40-500 μm with irregular shapes (Supplementary Figs. S1-S8). These areas are divided into grids with a spacing of 1 μm to ensure that those minerals larger than 1 μm can be identified, and then confirm the content (vol.%) of a mineral or melt by counting the number of squares it occupies (Table 1). Based on the relative content (vol.%) between the melt and plagioclase (partially transformed into maskelynite, which can be judged by the development of continuous

Always consult and cite the final, published document. See http:/www.minsocam.org or GeoscienceWorld

planar fractures and optical extinction), the spinel-bearing clasts can be divided into three types: S1, S2 and S3 (Table 1).

S1 type (53, accounting for 82.8% in 64 clasts) is the most common, in which the content of plagioclase ± maskelynite (48.8 vol.% – 80.9 vol.%, avg. 66.4 vol.%) is higher than that of the melt (14.7 vol.% – 42.2 vol.%, avg. 28.5 vol.%). The mafic-rich melt fills along the plagioclase fissure surface or intercrystal space, forming a lattice-like filling and interlocking textures (Figs. 3a-b). The spinels (0.2 vol.% – 5.2 vol.%, avg. 1.5 vol.%) occur as euhedral are incorporated into plagioclase containing mafic-rich melt (Fig. 3a). Mafic mineral ≤15.0 vol.%, only one clast with a spinel-bearing gabbro (No.14) containing ~15 vol.% olivine ± pyroxene (Table 1, Fig. S2).

The melt content (47.7 vol.% – 72.1 vol.%, avg. 58.6 vol.%) is more than that of plagioclase ± maskelynite (20.8 vol.% – 43.9 vol.%, avg. 35.9 vol.%) for the S2 type. The melt of S2 type has a finer and more uniform texture than S1 type, and it consists of nanoscale fine lines, honeycombs, fish-like scales and tail feathers (e.g., in the middle of Fig. 3c). Spinel and olivine ± pyroxene contents are 0.4 vol.% – 2.6 vol.%, avg. 1.1 vol.%, and 0.1 vol.% – 8.6 vol.%, avg. 4.3 vol.%, respectively. There are also spinel-bearing clasts that contain a large amount of impact melt pockets, molten veins, and mineral fragments, which are also classified as S2 type, and these phenomena further indicate the impact origin of the melt.

For S3 type, lath-shaped plagioclase and subhedral to euhedral spinels (1.6 vol.% – 2.2 vol.%) are dispersed in the homogeneous melt (52.8 vol.% – 70.3 vol.%, avg. 65.7 vol.%) and form a porphyritic texture (Figs. 3d). The average contents of spinel and olivine ± pyroxene are 1.8 vol.% and 0.56 vol.%, respectively. From S1, S2 to S3 type, the mixed degree between the melt and plagioclase increases, the content of plagioclase and mafic minerals decreases, the content of melt increases, and the content of spinel shows no significant change (Table 1).

FANs clasts are mainly composed of plagioclase (≥ 95 vol.%, An$_{95.5-97.6}$, avg. Mg$^{\#}$ = 39.6) (Supplementary Table S1-1). Shock-induced planar fractures appear in the plagioclase, containing finely dispersed dark mineral inclusions (Fig. S1). MANs clasts are composed of lath-like euhedral plagioclase crystals (An$_{93.4-97.7}$, avg. Mg$^{\#}$ = 56.5) (Table S1-2), olivine and pyroxene and a small amount of impact melt (Fig S2). There is no clear boundary between MANs clasts and spinel-bearing clasts. In addition to containing spinel, the distinctive feature of spinel-bearing clasts is that most plagioclases (An$_{90.9-96.8}$, Mg$^{\#}$=55.4, Table S1-3) have been converted into maskelynite by impact. Sorting by Mg$^{\#}$ value from highest to lowest: MANs ＞ spinel-bearing clasts ＞ FANs, whereas sorting by An value from highest to lowest: FANs ＞ MANs ＞ spinel-bearing clasts (Table 2). Among them, spinel-bearing clasts and MANs have similar plagioclase compositions.

Melt

All spinel-bearing clasts contain Mg-Al-rich melts. The occurrence of melts is closely related to spinel and plagioclase. Based on the relationship of occurrence and composition analysis, it is assumed that these melts are derived from impact melting and mixing of mafic minerals and plagioclase. To represent the precursor material properties of mixed melts, the concept of M value is introduced.

M value = (FeO+MgO) / Al_2O_3, wt.%.

The whole rock M value of a lunar meteorite is an important criterion for classifying lunar lithologies (M ≥ 1, mainly mare basalt; M < 1, mainly highland lithologies; this standard is obtained through statistics of 446 lunar meteorites published by the Meteoritical Bulletin, URL: www.lpi.usra.edu/meteor). The concept of M value is applicable to both chemical properties of melts and the determination of lunar rock types. The M value is a further promotion and improvement of previous foundation (Korotev et al., 2003). If M ≥ 1, it means that the melt mainly originates from mafic minerals; if M ＜ 1, it means that the melt mainly originates from plagioclase (Table 2). According to the above definitions, melt in spinel-bearing clasts can be divided into two types: one is relatively enriched in FeO + MgO (M = 6.17 – 30.5, avg. 15.9; Mg$^{\#}$ = 55.9 – 86.3, avg. 67.5, Table S1-4). The other is relatively enriched in Al_2O_3 (M = 0.17 – 0.89, avg. 0.39, Table S1-5) .

Always consult and cite the final, published document. See http:/www.minsocam.org or GeoscienceWorld

The melt shows no fixed shape and is divided into three types according to the occurrence: a. the melt looks like filled in interstitial or crack between plagioclase crystals (M1, Fig. 3b). b. fine lines and veins (M2, Fig. 3c). c. completely melted (Fig. 3d). M1 is mainly a mafic melt ($M \geq 1$), M2 contains both melts (mafic-rich melt and Al-rich melt), and M3 is mainly a melt with a high degree of mixing. Taking the spinel as the center, from the core to rim are mafic-rich melt, Al-rich melt and plagioclase (Figs. 3e-f). Compared to the plagioclase, the Al content in the melt containing spinel is significantly lower (Fig. 3g), and the content of Mg is significantly higher (Fig. 3h). The Al-rich melt is closely related to plagioclase, which is manifested by the partial melting and recrystallization of plagioclase (Fig. 3i). The mafic-rich melt is distributed in parallel bands in the plagioclase (Fig. 3j). The Mg-Al-rich melt, the mafic melt and plagioclase are interwoven (Fig. 3k). The spinel with a inclusion of silica-enriched glass crystallizes first in a Mg-Al-rich melt, it shows that rapid quenching and unbalanced crystallization (Fig. 3l). Abundance statistics of the different phases in 64 spinel-bearing clasts can be found: there is a clear inverse correlation between melt content and plagioclase content, and spinel content and olivine ± pyroxene content also have s similar inverse correlation (Fig. 4).

Spinel

Most spinels are euhedral to subhedral, with a particle size of 1 μm to 10 μm, and the maximum size does not exceed 15 μm (Figs. S1-S8). According to the composition, The spinel can be divided into a main group and a subgroup. The main group is rich in magnesium and aluminum ($Mg^{\#} = 89.2 – 93.1$, avg. 90.7; $Al^{\#} = 95.2 – 98.8$, avg. 97.4, Table S1-7). The subgroup has a higher content of Cr and Fe (avg. $Mg^{\#} = 55.5$, $Al^{\#} = 77.1$, Table S1-8) compared to the main group (Fig. 5a). The main group spinel has a weak growth zonation from core (avg. $Mg^{\#} = 91.3$) to rim (avg. $Mg^{\#} = 90$) (Table 2, Figs. 3a, 5b). Three types of spinel-bearing clasts (S1, S2 and S3) have the similar spinel composition. The $Mg^{\#}$ value of the main group is consistent with laboratory studies that connect mineral composition ($Mg^{\#} > 88$) to spectroscopic observations (Jackson et al., 2014), and the $Al^{\#}$ value is close to the experimental results of mineral spectroscopy simulation ($Al^{\#} > 99$, Williams et al., 2016). Some of the main group spinel cores are subgroup spinel, mainly Cr-Fe-spinel ($Mg^{\#} = 18.2 – 19.0$, $Al^{\#}=30.7 – 30.8$), e.g., Clasts No. 28 (Fig. 3f).

Olivine and pyroxene

The content of olivine ± pyroxene in 49 of spinel-bearing clasts is not more than 5 vol.% (avg. 1.9 vol.%, Table 1), which is consistent with the remote sensing definition of PSA (Pieters et al., 2011). The content of olivine ± pyroxene in the remaining 15 spinel-bearing clasts is greater than 5 vol.%, avg. 8.4 vol.%, which is similar to the previous definition of PST (e.g., Prinz et al., 1973; Marvin et al., 1989). Olivine in basaltic clasts is relatively iron-rich ($Mg^{\#} = 35.4$, Table S1-9), while olivine in MANs (Table S1-10) and spinel-bearing clasts (Table S1-11) are relatively magnesium-rich ($Mg^{\#} = 68.7$, 66.7, respectively, Table 2). Olivine in spinel-bearing clasts may have undergone different degrees of impact melting. The olivine is filled with nano-sized melt (Fig. 6a). Compared to olivine in basaltic and MANs clasts (avg. $Al_2O_3 = 0.29$ wt.%, 0.23 wt.%, M value = 220, 275, respectively), the olivine-melt from spinel-bearing clasts is obviously enriched in Al (avg. $Al_2O_3 = 1.77$ wt.%, M value = 51.2, Table S1-11), indicating that Al element entered the olivine-melt. The Raman peak positions of the olivine-melts have the characteristics of amorphous glass, while olivines in basaltic and MANs clasts are not obvious change compared with the standard Raman peaks of olivine (Fig. 6b). The pyroxene composition varies greatly, including low-Ca pyroxene ($Fs_{19.5\text{-}45.7}Wo_{1.97\text{-}4.21}$, Table S1-12), pigeonite ($Fs_{22.5\text{-}45.2}Wo_{5.64\text{-}20.7}$, Table S1-13) and high-Ca pyroxene ($Fs_{7.45\text{-}28.2}Wo_{26.2\text{-}42.8}$, Table S1-14). Most of the low-Ca pyroxenes contain lamellar exsolutions of high-Ca pyroxene (Fig. 6a).

Bulk composition and trace elements

The bulk major element compositions of NWA 13191 are determined by the NMFB method, using the average value of 20 analysis spots . The bulk $Mg^{\#}$ ranges from 88.1 to 91.9, avg. 89.8, M value is 0.22-0.24 (Table S2). The spinel-bearing clasts average bulk $Mg^{\#}$ and M value are 67, 0.62, respectively (Table S3). The chondrite-normalized

Always consult and cite the final, published document. See http:/www.minsocam.org or GeoscienceWorld

This is the peer-reviewed, final accepted version for American Mineralogist, published by the Mineralogical Society of America.
The published version is subject to change. Cite as Authors (Year) Title. American Mineralogist, in press.
DOI: https://doi.org/10.2138/am-2022-8728. http://www.minsocam.org/

rare earth element (REE) patterns of plagioclase in all clasts have LREE > HREE with positive Eu anomalies (δEu = 10.8 ± 4.51 for MANs, 15.1 ± 2.51 for FANs)(Table S4, Fig. 7a), it is similar to that of lunar meteorite MANs (Xu et al., 2020) and Apollo FANs (Papike et al., 1997; Floss et al., 1998) . ΣREE of the olivine (10.5 ppm) is much lower than that of the olivine-melt (avg. 55.2 ppm) (Fig. 7b). The chondrite-normalized REE pattern of the whole rock has slightly LREE > HREE with positive Eu anomalies (δEu = 1.41) (Table S4, Fig. 7c). The total amount of trace elements (avg., ppm), excluding REEs, in descending order is: olivine-melt (656), whole rock (431), spinel-bearing clasts (135), olivine (69.7), plagioclase in MANs (37.6), pyroxene (28.8), plagioclase in FANs (5.91) (Table S5).

Discussion

Evidence of the lunar origin of NWA 13191 meteorite

NWA 13191 is a polymict spinel-bearing breccia (Figs.1 and 2). The extensive development of impact melt indicates its identity as a meteorite. The main evidence for its lunar origin is as follows: a. The Fe/Mn (atom) ratio of olivine (84.3 – 131, avg. 104 for FANs; 82.5 – 125, avg. 96.8 for MANs; 67.0 – 141, avg. 101 for spinel-bearing clasts; Tables S1-9 – S1-11) and pyroxene (35.9 – 85.1, avg. 58.0, Table 2) are on the lunar trend line, different from Martian and HED meteorites (Figs. 8a and 8b). The deviation of individual data from the lunar trend line may be due to the fact that shock changes the crystal structure of olivine, while Fe^{2+} or Mn^{2+} has different M_2 position priorities in pigeonite (Cameron and Papike, 1981). b. The An value of plagioclase is the criterion for judging the evolution of planetary geology, and plagioclase from the Earth, Moon, Mars and Vesta has different An and K (afu) trends (Papike, 1998). The An value of NWA 13191 (avg. 95.4 – 96.6, Table 2) is higher than that of HED (66 – 96, Mittlefehldt, 2014) and Martian meteorites, and the range of variation is much smaller than that of HED and Martian meteorites. (Fig. 8c). c. Most of M values of melts fall on the line of the mare basalt (average value for "olivine + pyroxene + ilmenite") and highland anorthosite (Fig. 8d). Some data are close to the highland anorthosite, which represents the composition of anorthosite breccia, and other data are close to lunar basalt, which represents the composition of mafic melt or basaltic clasts. At the same time, there are two abnormal distribution clusters: one is an Al-Mg-rich melt (Al_2O_3 = 31.3 ± 12.3 wt.%, MgO = 11.2 ± 5.6 wt.%), and this melt can possibly form spinel; the other is Al-poor and rich in mafic components (Al_2O_3 = 3.3 ± 1.7 wt.%, MgO = 23.4 ± 6.9 wt.%, FeO = 20.5 ± 8.0 wt.%), which may be derived from impact melting of mafic minerals. d. The composition of spinel is within the range of spinel in PSA discovered by M^3 remote sensing data (Fig. 5, Prissel et al., 2014), which is the same as the trend range of spinel in Luna 20 soil (Fig. 9a, Keil et al., 1970; Cohen et al., 2001), suggesting that they may have a similar genesis.

The spinel-bearing clasts of NWA 13191 vs the spinel-bearing troctolite 2003 of Luna 20

According to the compositional and spectral analyses of the spinels synthesized, remote sensing defined PSA is consistent with spinel having $Mg^\# > 88$ (Jackson et al., 2014) and $Al^\# > 99$ (Williams et al., 2016). Among all lunar samples, spinel compositions basically meet the characteristics of PSA only for NWA 13191 and returned soil samples Luna 20 (Figs. 5 and 9a, Prinz et al. 1973; Wittmann et al., 2019). For further comparison, we compiled analytical data for Luna 20 samples (Bansal et al., 1972; Haggerty, 1973; Helmke et al., 1973; Prinz et al., 1973; Vinogradov, 1973; Snyder et al., 1992). We found that NWA 13191 and Luna 20 samples share the same types of clasts, such as PST, norite, basalt, and anorthosite, and similar mineral compositions. The anorthosite, spinel-bearing anorthosite and the whole rock of NWA 13191 and Luna 20 have mostly consistent major element compositions (Fig. 9b, Vinogradov, 1973). In terms of trace element content, the spinel-bearing clasts and whole rock compositions of NWA 13191 have the same range of REEs and other trace element concentration ranges as the soil particles from Luna 20, e.g., Sm, Sc and La (Figs. 9c and 9d). Therefore, the spinel-bearing clasts in NWA 13191 may have the similar origin as the spinel-bearing troctolite 2003 from Luna 20. Could the micron-scale spinel-bearing lithologies represent the PSA found by a spatial resolution of 140 – 280 m/pixel M^3 (Pieters et al., 2009)? The answer is "No". However, these spinel-bearing clasts have the same mineral chemical composition as PSA, which provides a possibility for its genesis.

Always consult and cite the final, published document. See http:/www.minsocam.org or GeoscienceWorld

The petrological type of spinel-bearing clasts in NWA 13191

The lunar crust is composed of numerous igneous rocks, including FANs, Mg-rich rocks (Papike et al., 1998) and mare basalts. FANs typically are composed of > 90 vol.% plagioclase rich in calcium (An > 96, Dowty et al., 1974a, 1974b), pyroxene and olivine that are relatively iron-rich ($Mg^{\#} < 70$). Mg-rich rocks are a lithologically diverse group (Shearer et al., 2015 and references therein). Papike et al. (1998) subdivided Mg-rich highland rocks into Mg-suites, alkaline suites and KREEP lithologies [lunar components rich in potassium (K), rare earth elements (REEs), and phosphorus (P)]. The Mg-suites include ultramafics (e.g., dunites, pyroxenites and harzburgites), PST, troctolites, anorthositic troctolites, norites and gabbronorites (Papike et al., 1998; Shearer et al., 2006). FANs, mare basalt and KREEP basalt have significantly different Ti/Sm and Sc/Sm ratios from Mg-suite lithologies and spinel-bearing clasts in NWA 13191, the $Mg^{\#}$ between them is also different (Figs. 10a-b, Fig. 11a). The Mg-suite and spinel-bearing clasts are very Mg-rich silicates (Figs. 10a-e) and have relatively high abundances of incompatible trace elements (e.g., REEs, Th, Y, Sc) compared with FANs (Figs. 9c, 10b-c, 11b, Table S5), however, they are significantly lower than those of KREEP basalts or quartz monzodiorites (QMD) (Fig. 10c). REEs and Th element are mainly concentrated in the residual phases of highly evolved magmas, and the representative lithologies are KREEP basalts or QMD. Using the partitioning behavior of Th between mafic silicates (pyroxene, olivine) and basaltic melt, the calculated Th contents of parent melts are similar to those of KREEP basalts (Hagerty et al. 2006). Although the $Mg^{\#}$ of mafic silicates, Mg-suite and spinel-bearing clasts in NWA 13191, is higher than that of the mare basalts, Cr_2O_3 (wt.%), Ni and Co concentrations are generally lower in the Mg-suite and spinel-bearing lithologies than those in the mare basalts (Figs. 10d-f). The Mg-suite rocks represented by PST, troctolites and anorthositic troctolites have similar ranges of $Mg^{\#}$ and trace element concentrations as spinel-bearing clasts in NWA 13191, indicating that they are derived from the same or similar magma sources.

Based on constraints on key features of PSA lithologies modified from Taylor and Pieters, 2013: (1) spinel-bearing clasts in NWA 13191 contain 0.2 – 5.2 vol.% (avg. 1.5 vol.%) spinel, slightly less than the ~ 5 – 8 vol.% assumed for the spinel base on spectral mixing experiments; 20.8 – 80.9 vol.% (avg. 60.9 vol.%) plagioclase ± maskelynite, 14.7 – 72.1 vol.% (avg. 34.2 vol.%) mixed melt, cumulative average content of plagioclase and melt is greater than 95 vol.%; (2) 49 spinel-bearing clasts contain less than 5 vol.% olivine ± pyroxene, and 15 spinel-bearing clasts contain olivine ± pyroxene between 5 – 15 vol.%; (3) bulk composition of NWA 13191 have 1.13 wt.% FeO (Table S2), avg. $Mg^{\#} = 89.7$, and the spinel-bearing clasts have avg. 4.6 wt.% FeO (Table S3), have the features of a high-$Mg^{\#}$, low-FeO melt (Pieters et al., 2011). Among the 64 spinel-bearing clasts, 49 meet the index characteristics of PSA, but it is not clear if there is a large amount of melt in PSA defined by remote sensing (Pieters et al., 2011), because the melt, maskelynite (shocked plagioclase) or fine grained matrix (equivalent to mature lunar soil) does not have an obvious absorption peak and cannot be effectively identified by reflectance spectrum (Dhingra et al., 2011; Pieters et al., 2014). Based on the extensive development of impact melting on the lunar surface and the fact that most plagioclase are transformed into maskelynite, it is reasonable to speculate that at least some PSA lithologies contain a certain amount of melts. However, based on the definitive evidence currently available, the spinel-bearing clasts in NWA 13191 is different from both PST and PSA.

Formation of spinel-bearing clasts in NWA 13191

Since the first discovery of spinel-bearing clasts in Apollo samples, scientists have explored their formation, but have not formed an unified opinion (Gross et al., 2014 and references therein). The petrological characteristics and computational results of the isothermal, isobaric phase diagrams of enthalpy versus composition support recrystallization from impact melts (Treiman et al., 2015). Similarly, impact melting has been suggested as the mode of formation of fine-grained, glassy melt breccias in Dho 1528 and GRA 06157 that contain ＜10 - 20 μm spinel phenocrysts (Wittmann et al., 2019). The presence of spinel in meteorite NWA 13191 is closely related to melting, but is the origin of the melts caused by impact melting (exogenic) or magma (endogenic)? As the meteorite underwent

Always consult and cite the final, published document. See http:/www.minsocam.org or GeoscienceWorld

This is the peer-reviewed, final accepted version for American Mineralogist, published by the Mineralogical Society of America.
The published version is subject to change. Cite as Authors (Year) Title. American Mineralogist, in press.
DOI: https://doi.org/10.2138/am-2022-8728. http://www.minsocam.org/

complex impact deformation, it is difficult to distinguish on the basis of occurrence alone. It is necessary to rely on global judgments such as "occurrence + compositions". The melts invades along crystal planes, or other fracture of the plagioclase in NWA 13191, forming a reticulated filling texture (Fig. 3). The interlaced reticulated texture is a typical feature of the impact melt (e.g., Wittmann et al., 2019). The olivine (avg. $Mg^{\#} = 68.7$) in MANs and olivine-melt (avg. $Mg^{\#} = 66.7$) in spinel-bearing clasts have similar chemical compositions. The olivine in spinel-bearing clasts may have undergone metamorphic interactions with the aluminum-rich melt, resulting in its relatively high content of Al_2O_3 (1.77 ± 0.94 wt.%) (Table 2).

To obtain more information on the origin of the melt, we completed the analysis of trace elements such as REEs and incompatible elements *in situ* for plagioclase, olivine and spinel-bearing clasts. These results show that the REE distribution pattern of plagioclase is consistent with the previous analysis, and can be divided into FANs and MANs (Fig. 7a, Floss et al., 1998; Papike et al., 1997; Xu et al., 2020). The ΣREE of plagioclase in MANs (avg. 43.1 ppm) is higher than that of FANs (avg. 14.1 ppm), which may be the result of an evolved parental magma (e.g., Hess 1994; Papike et al., 1996; Shearer et al., 2015). It is particularly notable that the olivine-melt has a higher ΣREE (avg. 55.2 ppm) than the olivine in mare basalt, but is still lower than the olivine-enriched Mg-suite (Fig. 7b). The pattern of REE distribution in spinel-bearing clasts is consistent with that of the whole rock, and their ΣREE are much higher than those of plagioclase, pyroxene and olivine but slightly lower than that of the Mg-suite (Figs. 7b-c).

Liquidus equilibria in simple systems show that bulk rock compositions rich in olivine + plagioclase components will produce melts that crystallize spinel (Walker et al., 1973). Low-pressure experiments on natural Apollo samples indicate that such compositions could be produced by partial or complete melting of lunar crustal materials, not necessarily by partial melting of material from deep within the Moon (Walker et al., 1973). This would be equivalent to impact melting of troctolitic rocks. In this hypothesis, spinel-bearing rocks were formed from olivine-plagioclase melts produced by impact melting on or near the surface (Marvin and Walker, 1985). This scenario has been confirmed by low pressure experiments on plagioclase-olivine melting rates (Marvin and Walker, 1985) from natural samples. Using the bulk composition (Longhi et al., 2010) similar to the spinel-bearing clast No.63 of the meteorite NWA 13191 (Table S3), a subhedral to euhedral combination of "spinel (1 – 10 μm, $Mg^{\#} = \sim 94$, $Al^{\#} = \sim 95$) + anorthite + glass" has been formed under phase equilibrium conditions of 1 atm, f_{O2} (~IW-1), and 1300 °C (Prissel et al., 2016). Simulated crystallization experiments show that with a similar composition to the melt (forsterite + anorthite), up to 7.7 wt.% spinel ($Mg^{\#} = 91.3$) can be be crystallized at 1 bar, 1450 – 1350 °C, without any olivine and pyroxene formation (Gross et al., 2014). Under the same pressure and oxygen fugacity conditions on the Moon, as the temperature drops (1450 – 1150 °C), spinel crystallizes first, followed by calcium-rich plagioclase, Mg-rich olivine ($Mg^{\#} = 89.1 - 93.9$) and pyroxene crystallize in sequence (Gross et al., 2014). spinel-bearing clasts with plagioclase and melt as the main components, with a small amount of spinel and olivine, is the inevitable result of rapid quenching and unbalanced crystallization of the impact mixed melt.

In summary, the spinel-bearing clasts in NWA 13191 are consistent with the Mg-suite in terms of geochemical properties, particularly for PST, troctolites, anorthositic troctolites, MANs and olivine-rich rocks. However, spinel-bearing clasts contains a large amount of melt (14.7 – 72.1 vol.%, avg. 34.1 vol.%) and a small amount of spinels (< 1 – 15 μm, avg. $Mg^{\#} = 90.6$, $Al^{\#} = 97.5$, 0.19 – 5.18 vol.%, avg.1.45 vol.%, Table 1). These phenomena indicate that these spinel-bearing clasts may originate from the rapid quenching of Mg-rich troctolites or MANs after impact melting. The spinel and anorthite crystallize sequentially at 1450 – 1350 °C, no olivine and pyroxene crystallize at this stage.

IMPLICATIONS

NWA 13191 is a lunar spinel-bearing polymict breccia meteorite. The clast types, mineral compositions, whole rock major and trace element compositions are all similar to those of the soil samples returned by Luna 20, especially for the composition trend of spinel (e.g., spinel-bearing troctolite 2003, Cohen et al., 2001). Therefore, the spinel-

Always consult and cite the final, published document. See http:/www.minsocam.org or GeoscienceWorld

This is the peer-reviewed, final accepted version for American Mineralogist, published by the Mineralogical Society of America.
The published version is subject to change. Cite as Authors (Year) Title. American Mineralogist, in press.
DOI: https://doi.org/10.2138/am-2022-8728. http://www.minsocam.org/

bearing clasts in NWA 13191 may have an origin similar to that of the spinel-bearing troctolite 2003 from Luna 20. Luna 20 soil was collected from the South rim of the Crisium Basin. Meanwhile, the spinel-bearing lithologies have been detected near Crisium Basin (Moriarty et al., 2022; Simon et al., 2022). The comparative study between the spinel-bearing clasts in NWA 13191 and spinel-bearing Luna 20 lithics will be published in the future paper. The composition of the spinel (avg. $Mg^{\#} = 90.6$, $Al^{\#} = 97.4$) and bulk composition (high-$Mg^{\#}$, low-FeO) in the spinel-bearing clasts of NWA 13191 are basically consistent with the characteristics of PSA defined by remote sensing (Pieters et al., 2011). Massive mixed melts are discovered in spinel-bearing clasts. It is not clear whether a melt is present in the PSA speculated by remote sensing, as the melt or shocked plagioclase has no obvious absorption peak and cannot be effectively identified (Dhingra et al., 2011; Pieters et al., 2014). The simulated crystallization experiment proves that a large amount of melt can exist in rocks containing spinel + plagioclase (Gross et al., 2014). Therefore, the spinel-bearing clasts in NWA 13191 can be selected as one of the samples corresponding to the the PSA or PST lithologies, but no whole PSA lithology have been found for laboratory study so far.

Detailed information of the spinel-bearing clasts in NWA 13191 is obtained for the first time: in addition to plagioclase and newly formed spinel, a very small amount of mafic minerals and a large amount of Mg-Al-rich melt are found. There are three different occurrences and compositions of melts in the spinel-bearing clasts (M1, M2 and M3). The discovery of many mafic and mixed melts, and olivine-melt, indicates that the spinel-bearing clasts of NWA 13191 underwent partial melting and rapid disequilibrium crystallization. Only the spinel with a higher crystallization temperature is fully crystallized, and a small amount of forsterite and Mg-rich pyroxene crystallized in individual clasts (e.g., No. 2 clast in Fig. S1). Equivalent to the lunar impact melting conditions (1 bar), the temperature range for the formation of “spinel + plagioclase + glass” assemblage is 1450 – 1300 ℃ (Gross et al., 2014).

Lunar meteorite NWA 13191 records the highest bulk $Mg^{\#}$ (avg. 89.8) among the lunar samples thus far, higher than the next highest average value (82.0) of lunar meteorite NWA 10401 (Gross et al., 2020). The highly Mg-rich melt may be one of the conditions for spinel crystallization. The spinel in NWA 12279 has very high $Al^{\#}$ and $Mg^{\#}$ (avg., 97.4 and 90.6, max., 99.7 and 93.6, respectively). The chemical properties of spinel-bearing clasts in NWA 13191 are consistent with the slightly REE-enriched and alkali-poor Mg-suite rocks, such as PST, MANs, anorthositic troctolites and olivine-enriched Mg-suite rocks. However, most of the spinel-bearing clasts contain only a very small amount of mafic minerals, while a large amount of melt hosts some Mg-rich micro-spinels. These phenomena indicate that the spinel-bearing clasts in NWA 13191 are imbalanced crystalline product from rapidly quenched impact melts of Mg-rich troctolite or anorthosite precursors.

ACKNOWLEDGMENTS

This research is supported by National Natural Science Foundation of China grants (41866008), Guangxi Yong and Middle-aged Teacher Ability Improvement Project (2022KY0240) and Guangxi Scientific Base and Talent Special Projects (AD1850007). The authors would like to express their gratitude to EditSprings (https://www.editsprings.cn/) for the expert linguistic services provided, Axel Wittmann (Arizona State University) and Wenzhe Fa (Peking University) for constructive discussions of early manuscript drafts.

REFERENCES CITED

Bansal, B. M., Church, S. E., Gast, P. W., Hubbard, N. J., Rhodes, J. M., and Wiesmann, H. (1972) The chemical composition of soil from the Apollo 16 and Luna 20 sites. Earth and Planetary Science Letters, 17, 29–35.

Brown, R. W. (1977) A sample fusion technique for whole rock analysis with the electron microprobe. Geochimica et Cosmochimica. Acta, 41, 435–438.

Cameron, M., and Papike, J. J. (1981) Structural and chemical variations in pyroxenes. American Mineralogist, 66, 1–50.

Always consult and cite the final, published document. See http:/www.minsocam.org or GeoscienceWorld

This is the peer-reviewed, final accepted version for American Mineralogist, published by the Mineralogical Society of America.
The published version is subject to change. Cite as Authors (Year) Title. American Mineralogist, in press.
DOI: https://doi.org/10.2138/am-2022-8728. http://www.minsocam.org/

Cheek, L. C., and Pieters, C. M. (2014) Reflectance spectroscopy of plagioclase-dominated mineral mixtures: Implications for characterizing lunar anorthosites remotely. American Mineralogist, 99, 1871–1892.

Cohen, B. A., Snyder, G. A., Hall, C. M., Taylor, L. A., and Nazarov, M. A. (2001) Argon^{40}–argon^{39} chronology and petrogenesis along the eastern limb of the Moon from Luna 16, 20 and 24 samples. Meteoritics and Planetary Science, 36 (10), 1345–1366.

Dhingra, D., Pieters, C. M., Boardman, J. W., Head, J. W., Isaacson, P. J., and Taylor, L. A. (2011) Compositional diversity at Theophilus Crater: Understanding the geological context of Mg-spinel-bearing central peaks. Geophysical Research Letters, 38, L11201.

Dowty, E., Prinz, M., and Keil, K. (1974a) Ferroan anorthosite – A widespread and distinctive lunar lock type. Earth and Planetary Science Letters, 24, 15–25.

Dowty, E., Keil, K., and Prinz, M. (1974b) Igneous rocks from Apollo 16 rake samples. Proceedings of the 5th Lunar Science Conference. Geochimica et Cosmochimica Acta, Supp. 5, 431–445.

Feng, L., Lin, Y. T., Hu, S., Xu, L., and Miao, B. K. (2011) Estimating compositions of natural ringwoodite in the heavily shocked Grove Mountains 052049 meteorite from Raman spectra. American Mineralogist, 96, 1480–1489.

Floss, C., James, O. B., Mcgee, J. J., and Crozaz, G. (1998) Lunar ferroan anorthosite petrogenesis: clues from trace element distributions in FAN subgroups. Geochimica et Cosmochimica Acta, 62, 1255–1283.

Gross, J., Treiman, A. H., and Le, L. (2011) Unique spinel-rich lithology in lunar meteorite ALHA 81005: origin and possible connection to M^3 observations of the farside highlands. 42nd Lunar and Planetary Science Conference, abstract 2620#.

Gross, J., and Treiman, A. H. (2011) Unique spinel-rich lithology in lunar meteorite ALHA 81005: Origin and possible connection to M^3 observations of the farside highlands. Journal of Geophysical Research. 116 (E10009), 1–9.

Gross, J., Isaacson, P. J., Treiman, A. H., Le, L., and Gorman, J. K. (2014) Spinel-rich lithologies in the lunar highland crust: linking lunar samples with crystallization experiments and remote sensing. American Mineralogist, 99, 1849–1859.

Gross, J., Hilton, A., Prissel, T. C., Setera, J. B., Korotev, R. L., and Calzada-Diaz, A. (2020) Geochemistry and Petrogenesis of Northwest Africa (NWA) 10401: A new type of the Mg-suite rocks? Journal of Geophysical Research–Planets. 125, 1–24.

Haggerty, S.E. (1973) Luna 20: mineral chemistry of spinel, pleonaste, chromite, ulvöspinel, ilmenite and rutile. Geochimica et Cosmochimica Acta, 37, 857–867.

Hagerty, J. J., Shearer, C. K., and Vaniman, D. T. (2006) Heat-producing elements in the lunar mantle: Insights from ion microprobe analyses of lunar pyroclastic glasses. Geochimica et Cosmochimica Acta, 70, 3457–3476.

Helmke, P. A., Blanchard, D. P., Jacobs, J. W., and Haskin, L. A. (1973) Rare earths, other trace elements and iron in Luna 20 samples. Geochimica et Cosmochimica Acta. 37, 869–874.

Herzberg, C. T., and Baker, M. B. (1980). The cordierite to spinel-cataclasite transition: structure of the lunar crust. Proc. Conf. Lunar Highlands Crust, 113–132.

Hess, P. C. (1994). Petrogenesis of lunar troctolites. Journal of Geophysical Research, 99 (E9), 19083–19093.

Hrstka, T., Gottlieb, P., Skála, R., Breiter, K., and Motl, D. (2018) Automated mineralogy and petrology – applications of TESCAN Integrated Mineral Analyzer (TIMA). Journal of Geosciences, 63 (1), 47–63.

Jackson, C. R. M., Cheek, L. C., Williams, K. B., Hanna, K. D., Pieters, C. M., Parman, S. W., Cooper, R. F., Dyar, M. D., Nelms, M., and Salvatore, M. R. (2014) Visible-infrared spectral properties of iron-bearing aluminate spinel under lunar-like redox condition. American Mineralogist, 99, 1821-1833.

Keil, K., Prinz, M., and Bunch, T. E., (1970) Mineral chemistry of lunar samples. Science, 167 (3918), 597–599.

Always consult and cite the final, published document. See http:/www.minsocam.org or GeoscienceWorld

This is the peer-reviewed, final accepted version for American Mineralogist, published by the Mineralogical Society of America.
The published version is subject to change. Cite as Authors (Year) Title. American Mineralogist, in press.
DOI: https://doi.org/10.2138/am-2022-8728. http://www.minsocam.org/

Korotev, R. L., Jolliff, B. L., Zeigler, R. A., Gillis, J. J., and Haskin, L. A., (2003) Feldspathic lunar meteorites and their implications for compositional remote sensing of the lunar surface and the composition of the lunar crust. Geochimica et Cosmochimica Acta, 67 (24), 4895–4923.

Liu, Y., Hu, Z., Gao, S., Günther, D., Xu, J., Gao, C., and Chen, H. (2008) *In situ* analysis of major and trace elements of anhydrous minerals by LA-ICP-MS without applying an internal standard. Chemical Geology, 257, 34–43.

Longhi, J., Durand, S. R., and Walker, D. (2010) The pattern of Ni and Co abundances in lunar olivines. Geochimica et Cosmochimica Acta, 74, 784–798.

Marvin, U. B., and Walker, D. (1985) A transient heating event in the history of a highlands troctolite from Apollo 12 soil 12033. Journal of Geophysical Research Solid Earth, 90, C421–C429.

Marvin, U. B., Carey, J. W., and Lindstrom, M. M. (1989) Cordierite-spinel troctolite, a new Mg-rich lithology from the lunar Highlands. Science, 243, 925–928.

Mittlefehldt, D.W. (2014) Asteroid (4) Vesta: I. The howardite-eucrite-diogenite (HED) clan of meteorites. Chemie der Erde-Geochemistry, 75, 155–183.

Morgan, Z., Liang, Y., and Hess, P. (2006) An experimental study of anorthosite dissolution in lunar picritic magmas: Implications for crustal assimilation processes. Geochimica et Cosmochimica Acta, 70, 3477–3491.

Moriarty, D. P., Simon, S. B., Shearer, C. K., Haggerty, S. E., Petro, N., and Li, S. (2022). Orbital assessment of the distribution and composition of spinel across the Crisium region: insights from luna 20 samples. 53rd Lunar and Planetary Science Conference, abstract 2139[#].

Papike, J. J., Fowler, G. W., Shearer, C. K., and Layne, G. D. (1996) Ion microprobe investigation of plagioclase and orthopyroxene from lunar Mg suite norites: Implications for calculating parental melt REE concentrations and for assessing post-crystallization REE redistribution. Geochimica et Cosmochimica Acta, 60, 3967–3978.

Papike, J. J., Fowler, G. W., and Shearer, C. K. (1997) Evolution of the lunar crust: SIMS study of plagioclase from ferroan anorthosites. Geochimica et Cosmochimica Acta, 61, 2343–2350.

Papike, J. J. (1998) Comparative planetary mineralogy: chemistry of melt-derived pyroxene, feldspar and olivine. Lunar and Planetary Science XXIX, abstract 1008[#].

Prinz, M., Dowty, E., and Keil, K. (1973) Mineralogy, petrology and chemistry of lithic fragments from Luna 20 fines: origin of the cummulate ANT suite and its relationship to high-alumina and mare basalts. Geochimica et Cosmochimica Acta, 37, 979–1006.

Pieters, C. M., Boardman, J., Buratti, B., Chatterjee, A., and White, M. (2009) The Moon Mineralogy Mapper (M^3) on Chandrayaan-1. Curr. Sci., 96, 500–505.

Pieters, C. M., Boardman, J., Buratti, B., Clark, R., Combe, J. P., Green, R., Goswami, J. N., Head, J. W., Hicks, M., Isaacson, P., Klima, R., Kramer, G., Kumar, K., Lundeen, S., Malaret, E., McCord, T. B., Mustard, J., Nettles, J., Petro, N., Runyon, C., Staid, M., Sunshine, J., Taylor, L. A., Thaisen, K., Tompkins, S., and Varanasi, P. (2010). Identification of a new spinel-rich lunar rock type by the Moon Mineralogy Mapper (M^3). 41st Lunar and Planetary Science Conference, abstract 1854[#].

Pieters, C. M., Besse, S., Boardman, J., Buratti, B., Cheek, L. C., Clark, R. N., Combe, J. P., Dhingra, D., Goswami, J., Green, R. O., Head, J.., Isaacson, P., Klima, R., Kramer, G., Lundeen, S., Malaret, E., McCord, T. B., Mustard, J. F., Nettles, J., Petro, N. E., Runyon, C., Staid, M., Sunshine, J., Taylor, L. A., Thaisen, K., Tompkins, S., and Whitte, J. L. (2011) Mg-spinel lithology: A new rock type on the lunar farside. Journal Geophys Research, E00G08, 1–14.

Pieters, C. M., Hanna, K. D., Cheek, L., Clark, R., Deepak, D., Prissel, T., Jackson, C., Moriarty, D., Parman, S., and Taylor, L.A. (2014) The distribution of Mg-spinel across the Moon and constraints on crustal origin. American Mineralogist, 99, 1893–1910.

Prinz, M., Dowty, E., Keil, K., and Bunch T. E. (1973) Spinel troctolite and anorthosite in Apollo 16 samples. Science,

Always consult and cite the final, published document. See http:/www.minsocam.org or GeoscienceWorld

This is the peer-reviewed, final accepted version for American Mineralogist, published by the Mineralogical Society of America.
The published version is subject to change. Cite as Authors (Year) Title. American Mineralogist, in press.
DOI: https://doi.org/10.2138/am-2022-8728. http://www.minsocam.org/

179, 74–76.

Prissel, T. C., Parman, S. W., Jackson, R. M., Rutherford, M. J., Hess, P. C., Head, J. W., Cheek, L. C., Dhingra, D., and Pieters, C. M. (2014) Pink Moon: The petrogenesis of pink spinel anorthosites and implications concerning Mg-suite magmatism. Earth and Planetary Science Letters, 403, 144–156.

Prissel, T. C., Parman, S. W., and Head, J. W. (2016) Formation of the lunar highlands Mg-suite as told by spinel. American Mineralogist, 101, 1624–1635.

Ridley, W. I., Reid, A. M., Warner, J., Brown, R. W., Gooley, R. and Donaldson, C. (1973) Major Element Composition of glasses in two Apollo 16 soils and a comparison with Luna 20 glasses. Lunar and Planetary Institute Science Conference Abstracts, 4, 625–627.

Shearer, C. K., Hess, P. C., Wieczorek, M. A., Pritchard, M. E., Parmentier, E. M., Borg, L. E., Longhi, J., Elkins-Tanton, L.T., Neal, C. R., Antonenko, I., Canup, R., Halliday, A. N., Grove, T. L., Hager, B. H., Lee, D. C., and Wiechert, U. (2006) Thermal and magmatic evolution of the Moon. Reviews Mineralogy and Geochemistry, 60, 365–518.

Shearer, C. K., Elardo, S. M., Petro, N. E., Borg, L. E., and McCubbin, F. M. (2015) Origin of the lunar highlands Mg-suite: An integrated petrology, geochemistry, chronology, and remote sensing perspective. American Mineralogist, 100, 294–325.

Simon, S. B., Shearer, C. K., Haggerty, S. E., Moriarty, D. P., Petro, N., Papike, J. J., and Vaci, Z. (2022). Multiple shallow crustal origins for spinel-bearing lithologies on the Moon: a perspective from the Luna 20 mission. Journal of Geophysical Research: Planets, 127(11), e2022JE007249.

Snyder, G. A., Taylor, L. A., and Neal, C. R. (1992) A chemical model for generating the sources of mare basalts: combined equilibrium and fractional crystallization of the lunar magmasphere. Geochimica et Cosmochimica Acta, 56, 3809–3823.

Sun, L. Z., Ling, Z. C., Zhang, J., Li. B., and Chen. J. (2016) The spectral characteristics and remote detection of lunar Mg-spinel: a case study of Tycho crater. SCIENTIA SINICA Physica, Mechanica & Astronomica, 46, 2, 029607.

Sun, Y., Li, L., and Zhang, Y. Z. (2017) Detection of spinel-bearing central peaks using M^3 images: Implications for the petrogenesis of Mg-spinel. Earth and Planetary Science Letters, 465, 48–58.

Taylor, L. A., and Pieters, C. M. (2013) Pink-spinel anorthosite formation: considerations for a feasible petrogenesis. 44^{th} Lunar and Planetary Science Conference, abstract $2758^{\#}$.

Treiman, A.H., Maloy, A.K., Shearer, C. K., and Gross, J. (2010) Magnesian anorthositic granulites in lunar meteorites in lunar meteorites Allan Hills 81005 and Dhofar 309: Geochemistry and global significance. Meteoritics and Planetary Science, 45, 163–180.

Treiman, A. H., Gross, J., and Glazner, A. F. (2015) Lunar rocks rich in Mg-Al spinel: Enthalpy constraints suggest origins by impact melting. 46^{th} Lunar and Planetary Science Conference, Abstract $^{\#}2518$.

Vinogradov, A. P. (1973) Preliminary data on lunar soil collected by the Luna 20 unmanned spacecraft. Geochimica et Cosmochimica Acta, 37, 721–729.

Walker, D., Longhi, J., Grove, T. L., Stolper, E., and Hays, J. F. (1973) Experimental petrology and origin of rocks from the Descartes Highlands. Proceedings of the 4^{th} Lunar Science Conference, 1013–1032.

Wittmann, A., Korotev, R. L., Jolliff, B. L., and Carpenter, P. K. (2019) Spinel assemblages in lunar meteorites Graves Nunataks 06157 and Dhofar 1528: Implications for impact melting and equilibration in the Moon's upper mantle. Meteoritics and Planetary Science, 54, 2, 379–394.

Williams, K. B., Jackson, C. R. M., Cheek, L. C., Donaldson Hanna, K. L., Parman, S. W., Pieters, C. M., Dyar, M. D., and Prissel, T. C. (2016) Reflectance spectroscopy of chromium-bearing spinel with application to recent orbital data from the Moon. American Mineralogist, 101, 726–734.

Always consult and cite the final, published document. See http:/www.minsocam.org or GeoscienceWorld

This is the peer-reviewed, final accepted version for American Mineralogist, published by the Mineralogical Society of America.
The published version is subject to change. Cite as Authors (Year) Title. American Mineralogist, in press.
DOI: https://doi.org/10.2138/am-2022-8728. http://www.minsocam.org/

Xu, X. Q., Hui, H. J., Chen, W., Huang, S. C., Neal, C. R., and Xu, X. S. (2020) Formation of lunar highlands anorthosites. Earth and Planetary Science Letters, 536,116238.

Zeng, X. J., Li, S. J., Li, X. Y., Wang, S. J., and Li, Y. (2015) Method for nondestructive measurement of major elements of lunar soil samples. Bulletin of Mineralogy, Petrology and Geochemistry, 34 (6), 1282–1286.

Zong, K. Q., Klemd, R., Yuan, Y., He, Z. Y., Guo, J. L., Shi, X. L., Liu, Y. S., Hu, Z. C., and Zhang, Z. M. (2017) The assembly of Rodinia: The correlation of early Neoproterozoic (ca. 900 Ma) high grade metamorphism and continental arc formation in the southern Beishan Orogen, southern Central Asian Orogenic Belt (CAOB). Precambrian Research, 290, 32–48.

Figure captions

FIGURE 1.

Appearance characteristics of NWA 13191 lunar meteorite (the sampling position is shown by the white dotted line).

FIGURE 2.

TESCAN result for thin section sample of NWA 13191, 2.

FIGURE 3.

Characteristics of spinel-bearing clasts in NWA 13191. (a) Clast No.13 is type S1; (b) The lattice-like filling and interwoven texture of type S1 for clast No. 9; (c) Clast No. 7 is type S2, note the fish scale interlacing texture on the left side (enlargement); (d) Clast No. 63 is type S3, Most spinel is embedded in the melt and a few in plagioclase. (e). BSE image (left) and corresponding Mg, Al, Ca, X-ray-intensity map (right) of clast No. 4, which shows the details of spinel in the mafic and Al-rich melt, and a large amount of lath-shaped plagioclase (2 – 10 μm) are distributed in the melt; (f). Cr-Fe-spinel is wrapped by a spinel with a compositional zonation; (g). X-ray-intensity map for aluminum of clast No.1 ; (h). X-ray-intensity map for magnesium of clast No.1. (i) Dissolution and recrystallization of plagioclase for clast No. 1; (j) The parallel veined mafic melts (M1) develop on the surface of plagioclase for clast No. 7; (k) Complete miscibility between mafic-melt and plagioclase for clast No. 4; (l) Differentiation of the elements after full miscibility for clast No. 36. Pl, Plagioclase; Mas, Maskelynite; Pyr, Pyroxene; Ol-M, Olivine-melt; Spi, spinel; Ilm, Ilmenite; Chr, Mg-Al-chromite; G, Glass debris; Si, silica-enriched glass; Mafic-M, Mafic-rich melt; Al-M, Al-rich melt; Mg-Al-melt, Mg-Al-rich melt; Im-Vein, Impact vein; M1, M2, and M3 correspond to impact melts for types S1, S2, and S3, respectively.

FIGURE 4.

Phase abundance (vol.%) in 64 spinel-bearing clasts.

FIGURE 5.

Plot of $Mg^{\#}$ vs. $Al^{\#}$ for spinels in spinel-bearing lithologies (a, Shearer et al., 2015 and references therein) and detailed composition information in NWA 13191 (b). The compositions of all the main group spinel in NWA 13191 are located in the solid gray box (b shows enlarged image), and the main group spinel has weak compositional zonation, which is relatively enriched in magnesium in the core and enriched in iron on the rim (other data are from Herzberg and Baker, 1980; Marvin et al., 1989; Cohen et al., 2001; Gross et al., 2014; Prissel et al., 2014; Wittmann et al., 2019).

FIGURE 6.

The characteristics of olivine and pyroxene in NWA 13191. (a) BSE image of spinel-bearing clast No. 16, olivine-melt and pyroxene are shown; (b) Olivine Raman spectra: b-1, olivine-melt; b-2, normal olivine ; b-3, standard Raman

Always consult and cite the final, published document. See http:/www.minsocam.org or GeoscienceWorld

spectrum of olivine from the RRUFF database (https://rruff.info).

FIGURE 7.

CI-chondrite normalized rare earth elements (REEs) distribution patterns for plagioclase, olivine, spinel-bearing clasts and whole-rock samples. (a) Plagioclase in MANs and FANs clasts. The plagioclase REE range of Apollo FANs (Papike et al., 1997; Floss et al., 1998) and lunar meteorite MANs clasts (Xu et al., 2020) is shown as gray and purple shaded areas, respectively, for comparison. (b) The olivine-melt have a relatively higher REEs content than olivine, but lower than that in olivine-enriched Mg-suite (lilac shaded areas, Shearer et al., 2015 and references therein). (c) Spinel-bearing clasts and the whole rock have the similar REEs distribution, which has a slightly lower than that of the olivine-poor Mg-suite (faint yellow shaded areas, Shearer et al., 2015).

FIGURE 8.

Key indicators of NWA 13191 meteorite originating from the moon. (a) Fe (afu) vs Mn (afu) of olivine; (b) Fe (afu) vs Mn (afu) of pyroxene; (c) An (afu) vs K(afu) of plagioclase (Papike, 1998); (d) Al_2O_3 (wt.%) vs FeO + MgO (wt.%) in the melts (Korotev et al., 2003); afu indicates atoms per formula unit based on 4 oxygen atoms for olivine, 6 for pyroxene and 8 for plagioclase.

FIGURE 9.

The comparison of chemical composition between NWA 13191 and Luna 20 soils. (a) Spinel composition trends; (b) Major elements in different clasts and whole rock; (c) Sc versus Sm; (d) La versus Eu. Luna 20 data is from Bansal et al. (1972); Haggerty, (1973); Helmke et al. (1973); Ridley et al. (1973).

FIGURE 10.

Ranges observed in a series of bulk geochemical parameters for lunar lithologies (Shearer et al., 2015 and references therein) and spinel-bearing clasts in NWA13191. (a) $Mg^{\#}$ vs. Ti/Sm. (b) $Mg^{\#}$ vs. Sc/Sm. (c) $Mg^{\#}$ vs. Th. (d) $Mg^{\#}$ vs. Cr_2O_3 wt.%. (e) $Mg^{\#}$ vs. Ni. (f) Co vs. Ni.

FIGURE 11.

Plot of major and trace elements in mafic silicates and melt (Shearer et al., 2015 and references therein). (a) $Mg^{\#}$ in mafic minerals or melt vs An in plagioclase of NWA 13191 and Mg-suite lithologies; (b) Y vs Ba in plagioclase of NWA 13191, KREEP basalts, FANs, mare basalts and Mg-suite lithologies.

Always consult and cite the final, published document. See http:/www.minsocam.org or GeoscienceWorld

This is the peer-reviewed, final accepted version for American Mineralogist, published by the Mineralogical Society of America.
The published version is subject to change. Cite as Authors (Year) Title. American Mineralogist, in press.
DOI: https://doi.org/10.2138/am-2022-8728. http://www.minsocam.org/

TABLE 1. Modal mineralogy of the spinel-bearing clasts (vol.%) in NWA 13191

No.	Pl+Mas	Melt	Spinel	Ol+Pyr	Others	Type	No.	Pl+Mas	Melt	Spinel	Ol+Pyr	Others	Type
1	40.99	57.92	1.00	0.10	N. D.	S2	33	42.19	47.65	1.56	8.60	N. D.	S2
2	20.77	72.11	0.56	6.23	0.34	S2	34	65.50	30.87	0.25	3.39	N. D.	S1
3	27.36	70.28	1.60	0.76	N. D.	S3	35	67.87	27.06	1.42	3.66	N. D.	S1
4	66.50	29.87	2.55	1.08	N. D.	S1	36	45.26	52.76	1.71	0.27	N. D.	S3
5	42.69	54.61	0.78	1.91	N. D.	S2	37	74.29	23.09	0.51	2.11	N. D.	S1
6	26.37	65.46	0.76	7.41	N. D.	S2	38	76.02	20.82	0.58	2.59	N. D.	S1
7	34.45	63.34	0.43	1.77	N. D.	S2	39	70.98	26.49	0.27	2.26	N. D.	S1
8	71.20	23.60	1.87	3.33	N. D.	S1	40	71.50	25.12	0.19	3.19	N. D.	S1
9	70.04	26.87	1.64	1.45	N. D.	S1	41	72.22	23.01	1.67	2.87	0.22	S1
10	67.57	29.81	0.65	1.96	N. D.	S1	42	55.66	39.37	0.41	4.55	N. D.	S1
11	62.12	36.54	0.72	0.62	N. D.	S1	43	74.40	24.25	0.72	0.62	N. D.	S1
12	57.39	37.79	1.42	3.40	N. D.	S1	44	70.59	27.70	0.45	1.26	N. D.	S1
13	67.44	30.01	1.78	0.77	N. D.	S1	45	68.80	20.17	2.53	8.50	N. D.	S1
14	55.76	28.70	1.20	14.33	N. D.	S1	46	69.57	20.78	4.38	5.28	N. D.	S1
15	52.74	39.75	1.21	6.30	N. D.	S1	47	59.82	38.16	1.47	0.55	N. D.	S1
16	60.08	37.69	1.69	0.54	N. D.	S1	48	69.49	26.52	2.50	1.50	N. D.	S1
17	65.75	31.55	0.49	2.21	N. D.	S1	49	71.83	22.68	1.96	3.53	N. D.	S1
18	55.40	42.21	1.16	1.24	N. D.	S1	50	66.14	32.28	0.75	0.82	N. D.	S1
19	61.74	30.73	0.91	6.61	N. D.	S1	51	71.40	23.51	1.95	3.14	N. D.	S1
20	65.82	15.46	1.56	14.95	2.21	S1	52	63.31	34.93	0.98	0.78	N. D.	S1
21	52.50	39.77	0.88	2.78	4.07	S1	53	72.15	23.34	1.65	2.86	N. D.	S1
22	70.78	21.03	0.47	7.72	N. D.	S1	54	63.47	32.70	2.17	1.67	N. D.	S1
23	48.84	37.03	0.96	13.17	N. D.	S1	55	74.70	15.74	0.63	8.92	N. D.	S1

Always consult and cite the final, published document. See http:/www.minsocam.org or GeoscienceWorld

This is the peer-reviewed, final accepted version for American Mineralogist, published by the Mineralogical Society of America.
The published version is subject to change. Cite as Authors (Year) Title. American Mineralogist, in press.
DOI: https://doi.org/10.2138/am-2022-8728. http://www.minsocam.org/

24	62.43	31.67	5.18	0.72	N. D.	S1	56	69.43	24.48	0.67	5.43	N. D.	S1
25	70.64	28.10	0.97	0.29	N. D.	S1	57	43.89	49.30	2.55	4.26	N. D.	S2
26	71.81	22.13	2.19	3.86	N. D.	S1	58	68.10	25.47	0.91	5.52	N. D.	S1
27	65.04	28.08	2.41	4.46	N. D.	S1	59	64.78	34.30	0.36	0.56	N. D.	S1
28	68.90	24.93	1.50	4.67	N. D.	S1	60	63.06	30.15	4.35	2.45	N. D.	S1
29	59.65	31.45	1.89	6.74	0.26	S1	61	60.36	38.27	0.78	0.60	N. D.	S1
30	71.08	27.27	0.21	1.39	0.05	S1	62	66.27	29.10	4.63	N. D.	N. D.	S1
31	73.70	25.61	0.69	N. D.	N. D.	S1	63	28.76	69.65	1.59	N. D.	N. D.	S3
32	80.89	14.65	2.78	1.68	N. D.	S1	64	26.33	70.24	2.24	1.19	N. D.	S3

No. is serial number of Mg-spinel-bearing clasts. Pl, Plagioclase; Mas, Maskelynite; Melt, mafic-rich , Al-rich and mixed melt; Ol ± Pyr, Olivine ± pyroxene; Other minerals include chromite, ilmenite, troilite and silica phase, etc. N. D. means not detected.

Always consult and cite the final, published document. See http:/www.minsocam.org or GeoscienceWorld

This is the peer-reviewed, final accepted version for American Mineralogist, published by the Mineralogical Society of America.
The published version is subject to change. Cite as Authors (Year) Title. American Mineralogist, in press.
DOI: https://doi.org/10.2138/am-2022-8728. http://www.minsocam.org/

TABLE 2. Major elements of minerals and melts in different clasts of NWA 13191

	Mineral or melt type	Plagioclase			Melt		Spinel			Olivine / olivine-melt			Pyroxene		
							Main group								
	Clast or mineral type	FANs	MANs	Mg-spinel bearing	Mafic-rich	Al-rich	core	rim	subgroup	Basalt	MANs	Mg-spinel bearing	Low-Ca	Pig	High-Ca
	N	16	12	33	23	52	16	14	3	9	7	43	8	17	20
oxide wt%	SiO_2	44.2 ± 0.78	44.4 ± 0.89	44.5 ± 0.78	44.6 ± 7.01	38.9 ± 12.9	0.24 ± 0.15	0.41 ± 0.26	0.25 ± 0.11	33.3 ± 2.01	36.5 ± 1.72	40.4 ± 2.73	52.1 ± 1.82	51.4 ± 1.47	52.2 ± 1.29
	TiO_2	0.02 ± 0.02	0.04 ± 0.04	0.03 ± 0.02	0.33 ± 0.37	0.25 ± 0.42	0.02 ± 0.02	0.04 ± 0.03	0.37 ± 0.04	0.07 ± 0.06	0.03 ± 0.03	0.07 ± 0.04	0.31 ± 0.10	0.52 ± 0.15	0.89 ± 0.35
	Al_2O_3	35.5 ± 1.35	35.0 ± 0.93	35.3 ± 1.13	3.32 ± 1.74	31.3 ± 12.3	66.9 ± 1.84	66.3 ± 1.59	44.7 ± 1.24	0.29 ± 0.14	0.23 ± 0.19	1.77 ± 0.94	0.85 ± 0.34	1.94 ± 1.02	1.92 ± 0.54
	Cr_2O_3	0.03 ± 0.05	0.03 ± 0.03	0.02 ± 0.03	0.21 ± 0.20	0.47 ± 0.86	2.63 ± 0.97	2.66 ± 0.91	19.8 ± 0.66	0.05 ± 0.03	0.03 ± 0.04	0.09 ± 0.09	0.30 ± 0.21	0.58 ± 0.27	0.51 ± 0.18
	FeO	0.35 ± 0.18	0.23 ± 0.05	0.33 ± 0.18	20.5 ± 8.02	4.88 ± 1.61	4.37 ± 0.51	4.95 ± 0.30	20.1 ± 0.41	49.3 ± 10.3	27.4 ± 5.89	26.3 ± 4.83	22.5 ± 5.46	19.8 ± 3.76	12.2 ± 3.48
	MnO	0.02 ± 0.03	0.02 ± 0.03	0.03 ± 0.04	0.22 ± 0.10	0.07 ± 0.05	0.05 ± 0.03	0.04 ± 0.04	0.17 ± 0.04	0.48 ± 0.14	0.23 ± 0.09	0.21 ± 0.10	0.35 ± 0.10	0.36 ± 0.06	0.22 ± 0.09
	MgO	0.14 ± 0.12	0.19 ± 0.11	0.25 ± 0.15	23.4 ± 6.93	11.16 ± 5.64	25.6 ± 0.84	24.9 ± 0.76	14.1 ± 0.24	15.6 ± 8.56	34.5 ± 4.19	26.3 ± 4.83	21.5 ± 4.26	19.3 ± 3.17	15.8 ± 2.04
	CaO	19.3 ± 0.86	19.3 ± 0.57	18.9 ± 0.69	6.32 ± 7.75	12.4 ± 4.74	0.17 ± 0.04	0.27 ± 0.31	0.31 ± 0.04	0.55 ± 0.25	0.32 ± 0.04	0.95 ± 0.4	1.61 ± 0.48	6.02 ± 2.51	16.1 ± 2.59
	Na_2O	0.29 ± 0.07	0.45 ± 0.16	0.43 ± 0.1	0.09 ± 0.06	0.34 ± 0.20	0.01 ± 0.02	0.02 ± 0.01	0.02 ± 0.02	0.04 ± 0.02	0.03 ± 0.02	0.05 ± 0.04	0.04 ± 0.02	0.05 ± 0.03	0.14 ± 0.15
	K_2O	0.03 ± 0.02	0.06 ± 0.05	0.05 ± 0.03	0.10 ± 0.14	0.06 ± 0.04	B. D.	0.01 ± 0.02	0.01	0.03 ± 0.01	0.02 ± 0.03	0.21 ± 0.17	0.01 ± 0.01	0.01 ± 0.02	0.02 ± 0.02
	NiO	0.01 ± 0.02	0.01 ± 0.01	0.01 ± 0.02	0.02 ± 0.02	0.02 ± 0.02	0.01 ± 0.02	0.01 ± 0.02	0.04 ± 0.04	0.01	0.03 ± 0.04	0.03 ± 0.03	0.01 ± 0.02	0.01 ± 0.02	0.02 ± 0.03
	Total	99.9 ± 0.52	99.7 ± 0.35	99.8 ± 0.46	99.1 ± 1.29	99.8 ± 0.89	100 ± 0.46	99.6 ± 0.84	99.8 ± 0.1	99.8 ± 0.2	99.4 ± 0.26	99.8 ± 0.29	99.6 ± 0.87	100 ± 0.49	100 ± 0.6
afu	Si	2.05 ± 0.04	2.06 ± 0.04	2.06 ± 0.4	6.82 ± 0.82	5.53 ± 1.82	0.01	0.01 ± 0.01	0.01	1 ± 0.01	0.99 ± 0.02	6.38 ± 0.29	1.96 ± 0.05	1.93 ± 0.03	1.95 ± 0.04
	Ti	B. D.	B. D.	B. D.	0.04 ± 0.04	0.03 ± 0.05	B. D.	B. D.	0.01	B. D.	B. D.	0.01	0.01	0.01	0.02 ± 0.01
	Al	1.94 ± 0.07	1.91 ± 0.05	1.93 ± 0.06	0.60 ± 0.32	5.26 ± 2.12	1.92 ± 0.24	1.92 ± 0.03	1.48 ± 0.04	0.01 ± 0.01	0.01 ± 0.01	0.33 ± 0.19	0.04 ± 0.01	0.09 ± 0.04	0.08 ± 0.02
	Cr	B. D.	B. D.	B. D.	0.03 ± 0.03	0.05 ± 0.1	0.05 ± 0.02	0.05 ± 0.02	0.44 ± 0.01	B. D.	B. D.	0.01 ± 0.01	0.01 ± 0.01	0.02 ± 0.01	0.01
	Fe	0.01 ± 0.01	0.01	0.01 ± 0.01	2.68 ± 1.14	0.58 ± 0.2	0.09 ± 0.01	0.1 ± 0.01	0.47 ± 0.01	1.25 ± 0.34	0.63 ± 0.15	3.5 ± 0.74	0.71 ± 0.19	0.62 ± 0.13	0.38 ± 0.11
	Mn	B. D.	B. D.	B. D.	0.03 ± 0.02	0.01 ± 0.01	0.01	B. D.	B. D.	0.1	0.01	0.04 ± 0.01	0.01	0.01	0.01
	Mg	0.01 ± 0.01	0.01 ± 0.01	0.02 ± 0.01	5.39 ± 1.69	2.38 ± 1.23	0.93 ± 0.03	0.91 ± 0.03	0.59 ± 0.01	0.69 ± 0.36	1.37 ± 0.14	6.98 ± 0.69	1.2 ± 0.2	1.07 ± 0.16	0.38 ± 0.11
	Ca	0.95 ± 0.04	0.96 ± 0.03	0.93 ± 0.04	1.01 ± 1.22	1.89 ± 0.71	B. D.	0.01 ± 0.01	0.01	0.02 ± 0.01	0.01	0.16 ± 0.07	0.06 ± 0.02	0.24 ± 0.1	0.64 ± 0.1
	Na	0.03 ± 0.01	0.04 ± 0.01	0.04 ± 0.01	0.03 ± 0.02	0.09 ± 0.06	B. D.	B. D.	B. D.	B. D.	B. D.	0.02 ± 0.01	B. D.	B. D.	0.01 ± 0.01
	K	B. D.	B. D.	B. D.	0.02 ± 0.03	0.01 ± 0.01	B. D.	B. D.	B. D.	B. D.	B. D.	0.04 ± 0.03	B. D.	B. D.	B. D.

Always consult and cite the final, published document. See http:/www.minsocam.org or GeoscienceWorld

This is the peer-reviewed, final accepted version for American Mineralogist, published by the Mineralogical Society of America.
The published version is subject to change. Cite as Authors (Year) Title. American Mineralogist, in press.
DOI: https://doi.org/10.2138/am-2022-8728. http://www.minsocam.org/

	Ni	B. D.	B. D.	B. D.	B. D.	B. D.	B. D.	B. D.	B. D.	B. D.	B. D.	B. D.	B. D.	B. D.	B. D.
	Total	5 ± 0.01	5 ± 0.01	5 ± 0.02	16.7 ± 0.68	15.8 ± 0.74	3 ± 0.01	3 ± 0.01	3 ± 0.01	2.99 ± 0.01	3.01 ± 0.02	17.5 ± 0.27	4.01 ± 0.04	4 ± 0.02	4 ± 0.03
evaluation parameter (avg.)	An/Fa/En	96.6 ± 0.7	95.6 ± 1.73	95.4 ± 1.1	N.A.	N.A.	N.A.	N.A.	N.A.	64.7 ± 18.3	31.3 ± 7.32	33.3 ± 6.33	60.6 ± 9.42	55.3 ± 7.83	46.1 ± 4.95
	Or/Wo	0.21 ± 0.11	0.33 ± 0.28	0.32 ± 0.18	N.A.	N.A.	N.A.	N.A.	N.A.	N.A.	N.A.	N.A.	3.25 ± 0.86	12.5 ± 5.3	33.9 ± 5.77
	Al#	N.A.	N.A.	N.A.	94.7 ± 5.38	99.3 ± 0.89	97.4 ± 0.98	97.4 ± 0.9	77.1 ± 1.07	86 ± 5.6	88 ± 10.5	96.4 ± 4.58	81.4 ± 9.43	82.2 ± 6.38	85.5 ± 3.91
	Mg#	N.A.	N.A.	N.A.	67.5 ± 8.02	78.2 ± 7.85	91.3 ± 0.91	90 ± 0.42	55.5 ± 0.11	35.3 ± 18.3	68.7 ± 7.32	66.7 ± 6.33	62.7 ± 10	63.2 ± 7.24	70 ± 7.73
	M value	0.01 ± 0.01	0.01	0.02 ± 0.01	15.9 ± 8.51	0.39 ± 0.22	0.45 ± 0.03	0.45 ± 0.02	0.76 ± 0.04	220 ± 92.3	275 ± 281	51.2 ± 77.3	62.7 ± 33.1	25.7 ± 13.6	16.4 ± 7.5
	Fe/Mn	N.A.	N.A.	N.A.	N.A.	N.A.	N.A.	N.A.	N.A.	104 ± 16.6	96.8 ± 16	101 ± 17.6	64.3 ± 9.32	54.4 ± 6.6	56.6 ± 15.0

N is the numbers of analysis spots. The "afu" indicates atoms per formula unit based on 4 oxygen atoms for olivine, 6 for pyroxene and 8 for plagioclase, 24 oxygen atoms for melt. 24 oxygen atoms are equal to the lowest common multiple of the oxygen atoms for plagioclase (8), olivine (4) and pyroxene(6). B. D. means below detection; N.A. means not applicable. The numbers following the "±" sign are the standard deviations of all analysis spots. The results of EPMA are better than 0.01%. An is afu [Ca / (Na + K + Ca)] × 100 for plagioclase; Ab is afu [Na / (Na + K + Ca)] × 100 for plagioclase; Or is afu [K / (Na + K + Ca)] × 100 for plagioclase; Fa is afu [Fe / (Mg + Fe)] ×100 for olivine; En is afu [Mg / (Mg + Fe + Ca)] ×100 for pyroxene; Wo is afu [Ca / (Mg + Fe + Ca)] × 100 for pyroxene. Al# is afu [Al / (Al + Cr)] × 100 for spinel; Mg# is afu [Mg / (Mg + Fe)] ×100 for spinel, olivine, pyroxene and melt; M value is express as (FeO + MgO)/Al_2O_3, wt.% for whole rock and mineral phase. Fe/Mn is afu Fe/Mn for olivines and pyroxenes. The olivine-melt (olivine has been transformed into vitreous) contains 0.11 wt. % – 4.80 wt. % Al_2O_3 and 0.42 wt. % – 1.95 wt. % CaO. Pig is pigeonite, a kind of pyroxene, Wo is 5 – 25 (afu).

Always consult and cite the final, published document. See http:/www.minsocam.org or GeoscienceWorld

This is the peer-reviewed, final accepted version for American Mineralogist, published by the Mineralogical Society of America.
The published version is subject to change. Cite as Authors (Year) Title. American Mineralogist, in press.
DOI: https://doi.org/10.2138/am-2022-8728. http://www.minsocam.org/

Fig. 1

Always consult and cite the final, published document. See http:/www.minsocam.org or GeoscienceWorld

This is the peer-reviewed, final accepted version for American Mineralogist, published by the Mineralogical Society of America.
The published version is subject to change. Cite as Authors (Year) Title. American Mineralogist, in press.
DOI: https://doi.org/10.2138/am-2022-8728. http://www.minsocam.org/

Fig. 2

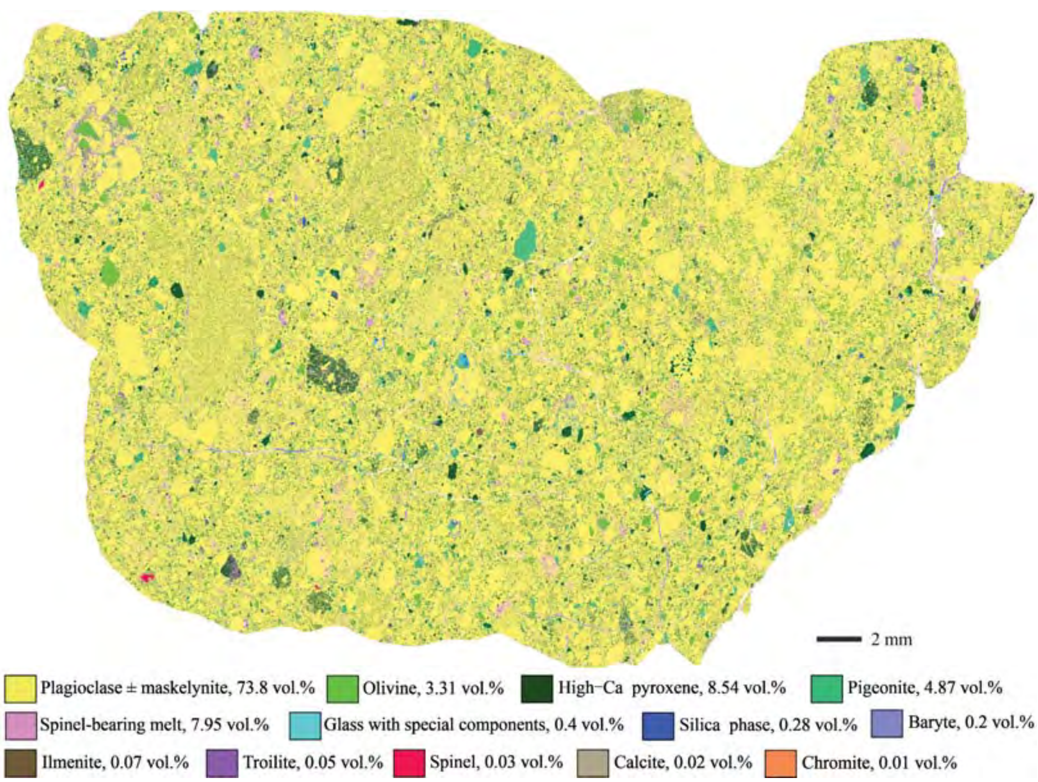

Always consult and cite the final, published document. See http:/www.minsocam.org or GeoscienceWorld

This is the peer-reviewed, final accepted version for American Mineralogist, published by the Mineralogical Society of America.
The published version is subject to change. Cite as Authors (Year) Title. American Mineralogist, in press.
DOI: https://doi.org/10.2138/am-2022-8728. http://www.minsocam.org/

Fig. 3

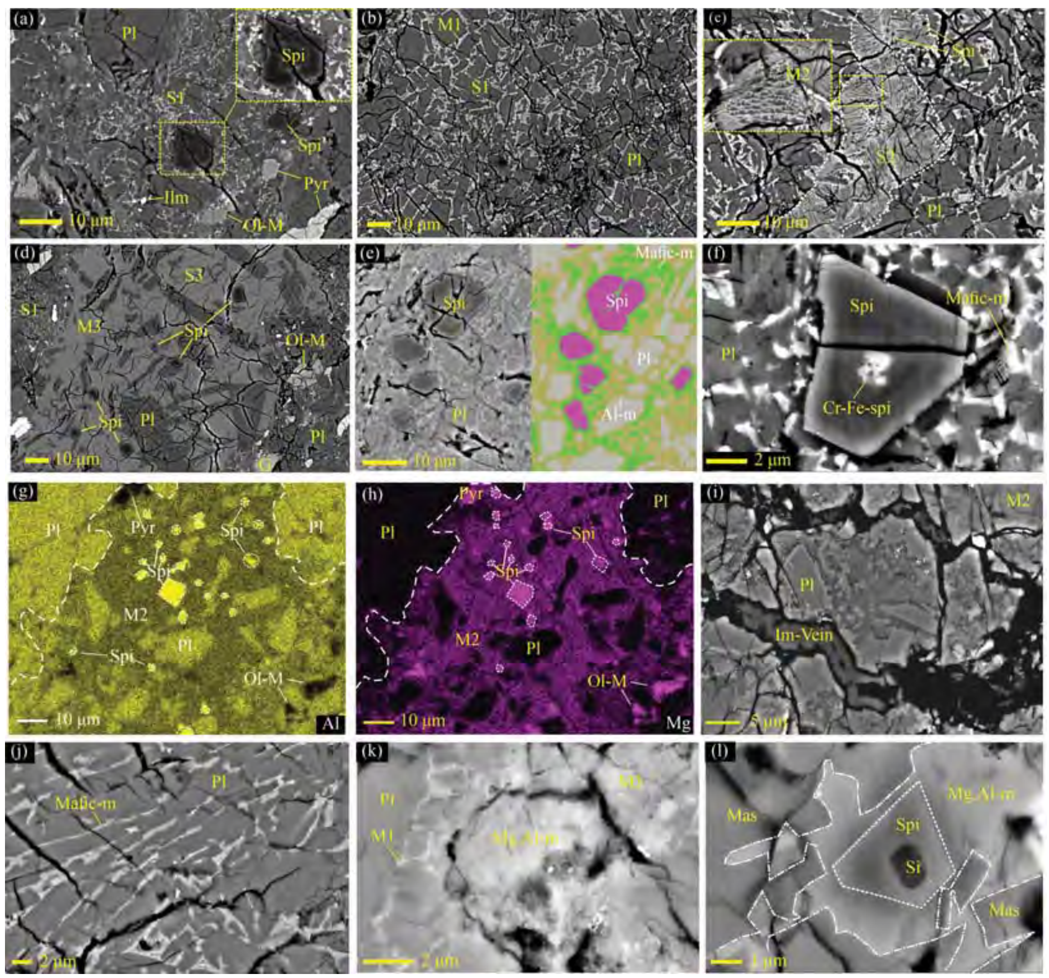

Always consult and cite the final, published document. See http:/www.minsocam.org or GeoscienceWorld

This is the peer-reviewed, final accepted version for American Mineralogist, published by the Mineralogical Society of America.
The published version is subject to change. Cite as Authors (Year) Title. American Mineralogist, in press.
DOI: https://doi.org/10.2138/am-2022-8728. http://www.minsocam.org/

Fig. 4

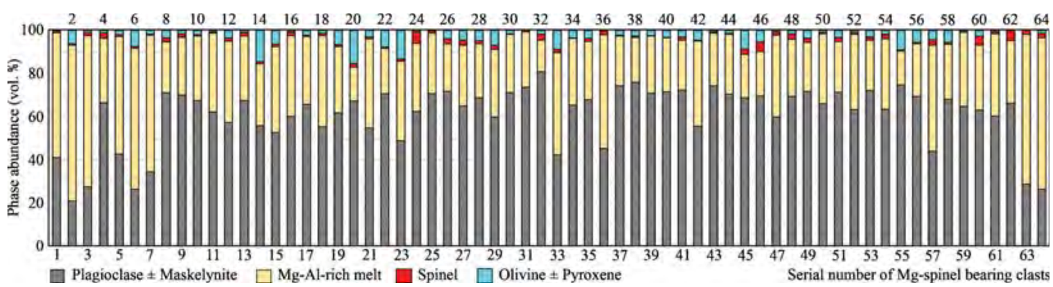

Always consult and cite the final, published document. See http:/www.minsocam.org or GeoscienceWorld

This is the peer-reviewed, final accepted version for American Mineralogist, published by the Mineralogical Society of America.
The published version is subject to change. Cite as Authors (Year) Title. American Mineralogist, in press.
DOI: https://doi.org/10.2138/am-2022-8728. http://www.minsocam.org/

Fig. 5

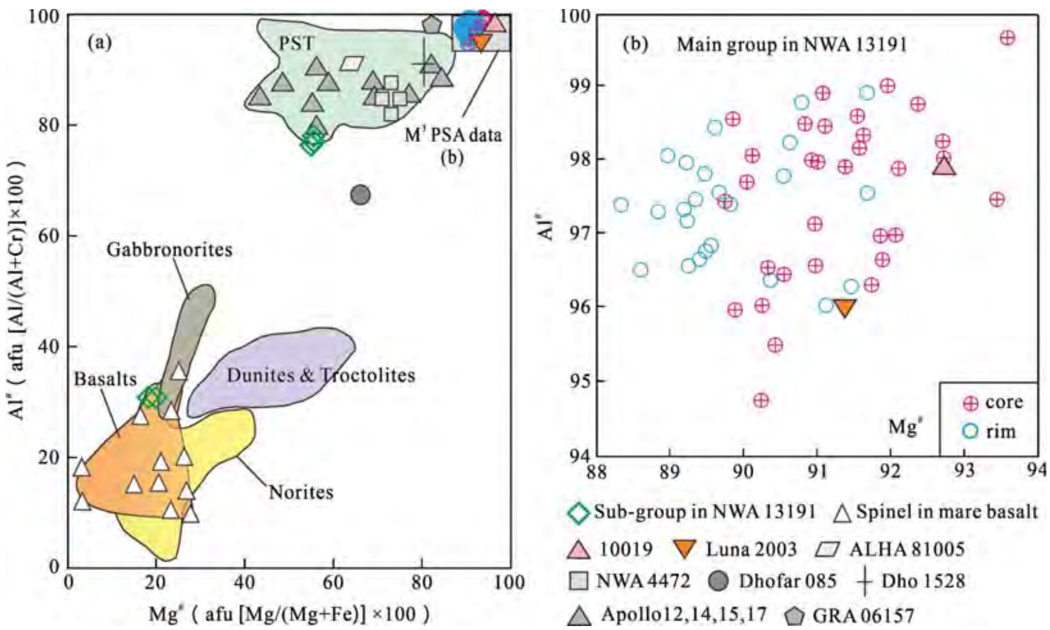

Always consult and cite the final, published document. See http:/www.minsocam.org or GeoscienceWorld

This is the peer-reviewed, final accepted version for American Mineralogist, published by the Mineralogical Society of America.
The published version is subject to change. Cite as Authors (Year) Title. American Mineralogist, in press.
DOI: https://doi.org/10.2138/am-2022-8728. http://www.minsocam.org/

Fig. 6

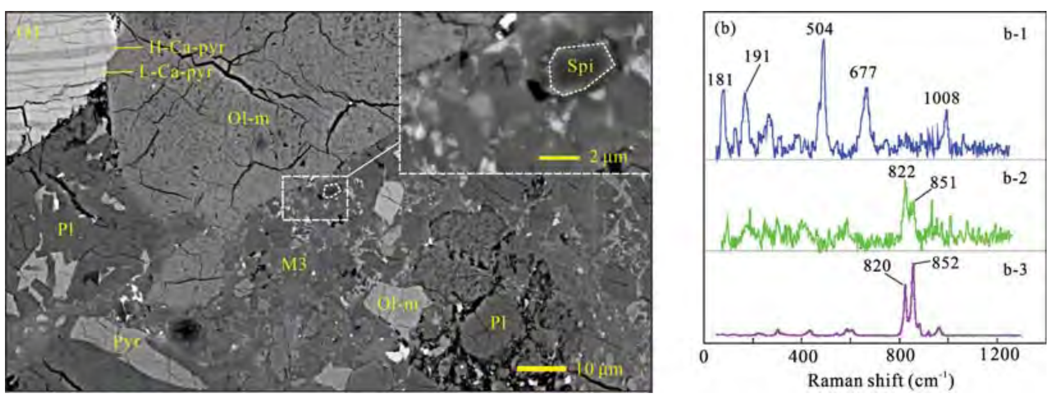

This is the peer-reviewed, final accepted version for American Mineralogist, published by the Mineralogical Society of America.
The published version is subject to change. Cite as Authors (Year) Title. American Mineralogist, in press.
DOI: https://doi.org/10.2138/am-2022-8728. http://www.minsocam.org/

Fig. 7

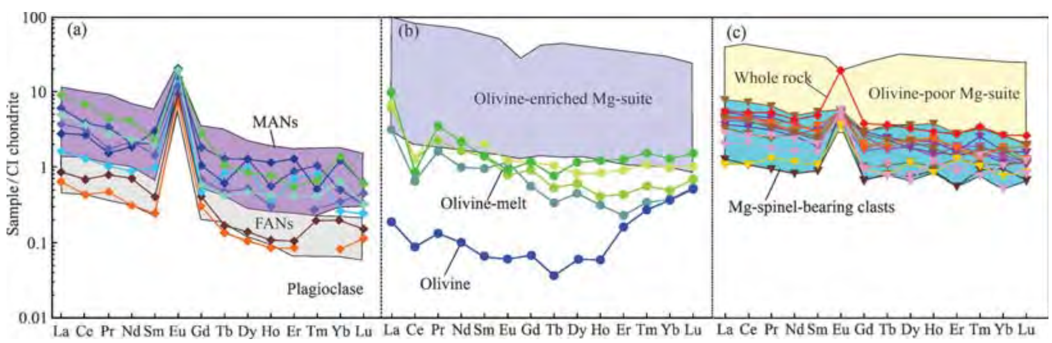

Always consult and cite the final, published document. See http:/www.minsocam.org or GeoscienceWorld

This is the peer-reviewed, final accepted version for American Mineralogist, published by the Mineralogical Society of America.
The published version is subject to change. Cite as Authors (Year) Title. American Mineralogist, in press.
DOI: https://doi.org/10.2138/am-2022-8728. http://www.minsocam.org/

Fig. 8

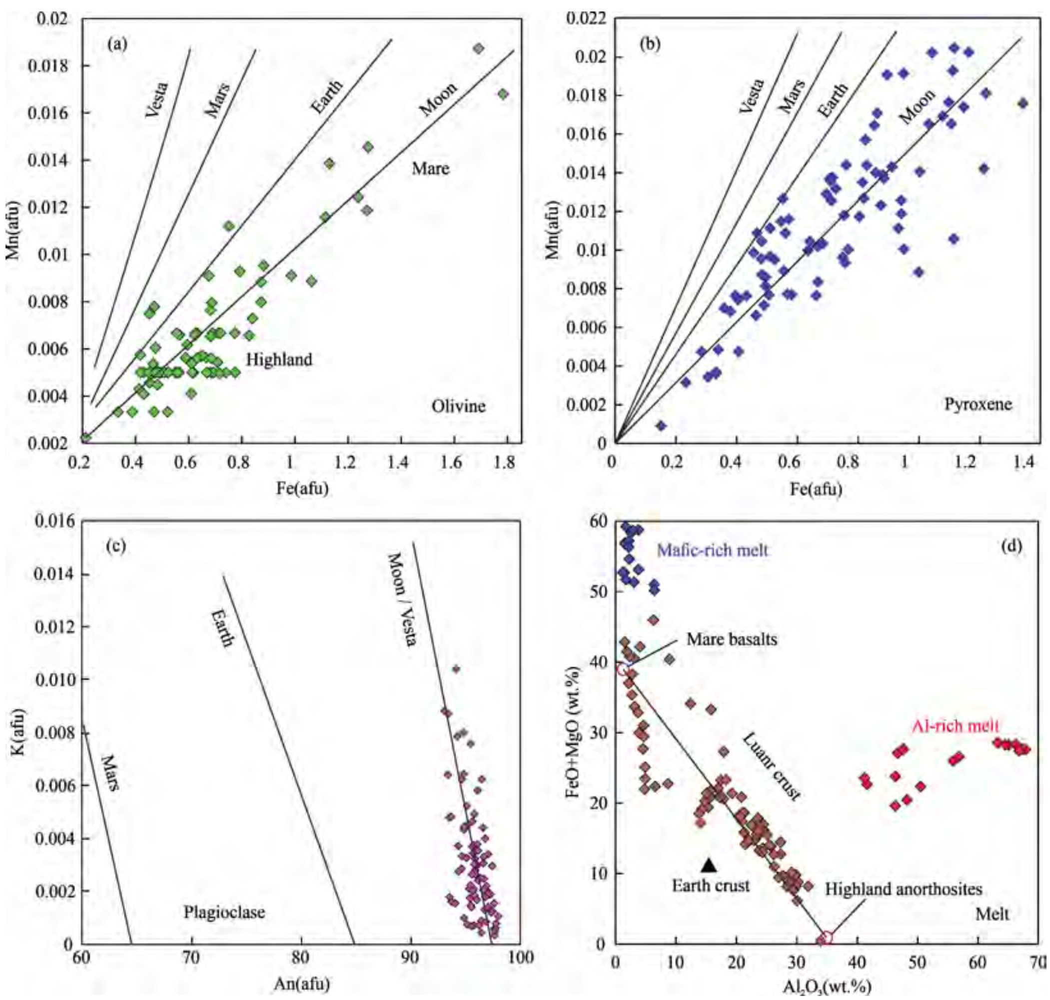

Always consult and cite the final, published document. See http:/www.minsocam.org or GeoscienceWorld

This is the peer-reviewed, final accepted version for American Mineralogist, published by the Mineralogical Society of America.
The published version is subject to change. Cite as Authors (Year) Title. American Mineralogist, in press.
DOI: https://doi.org/10.2138/am-2022-8728. http://www.minsocam.org/

Fig.9

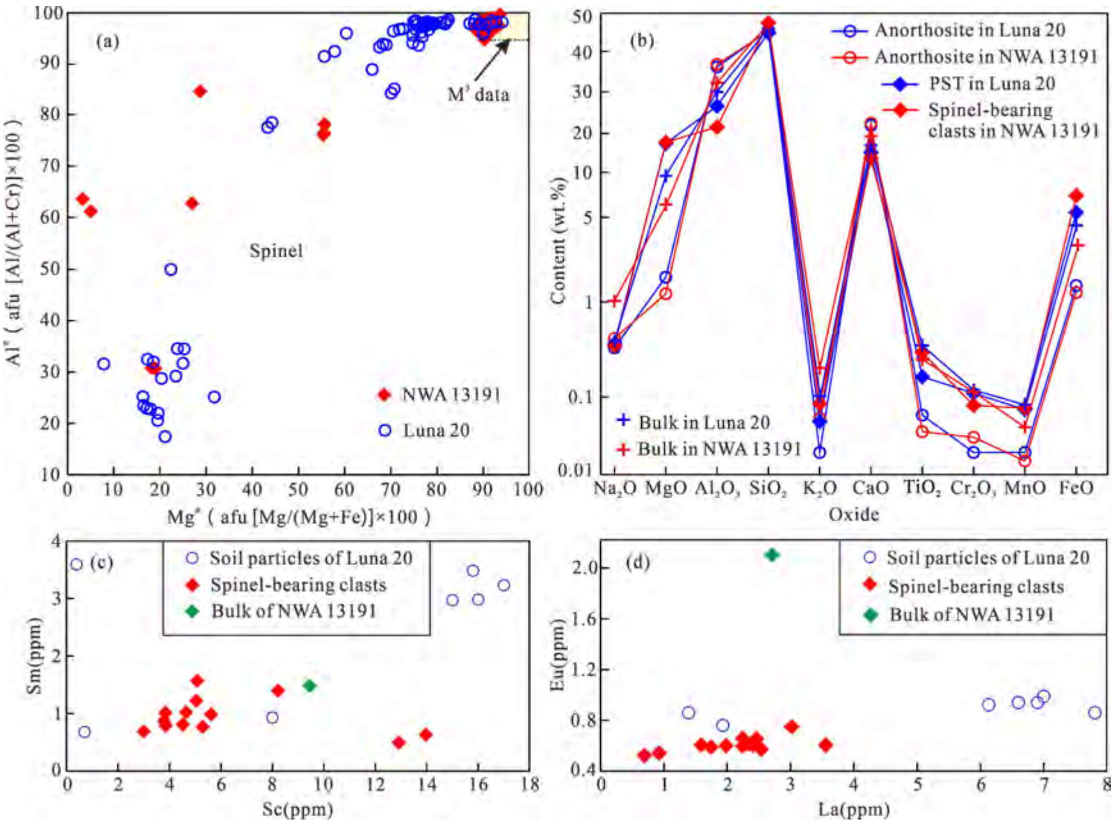

Always consult and cite the final, published document. See http:/www.minsocam.org or GeoscienceWorld

This is the peer-reviewed, final accepted version for American Mineralogist, published by the Mineralogical Society of America.
The published version is subject to change. Cite as Authors (Year) Title. American Mineralogist, in press.
DOI: https://doi.org/10.2138/am-2022-8728. http://www.minsocam.org/

Fig. 10

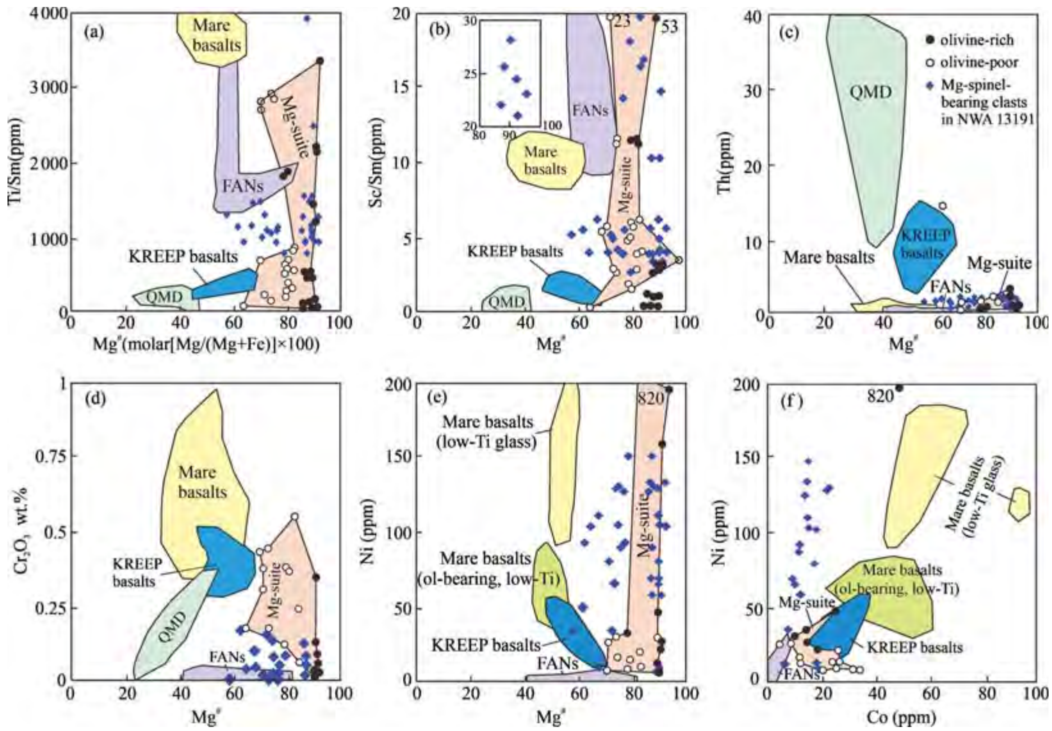

Always consult and cite the final, published document. See http:/www.minsocam.org or GeoscienceWorld

This is the peer-reviewed, final accepted version for American Mineralogist, published by the Mineralogical Society of America.
The published version is subject to change. Cite as Authors (Year) Title. American Mineralogist, in press.
DOI: https://doi.org/10.2138/am-2022-8728. http://www.minsocam.org/

Fig. 11

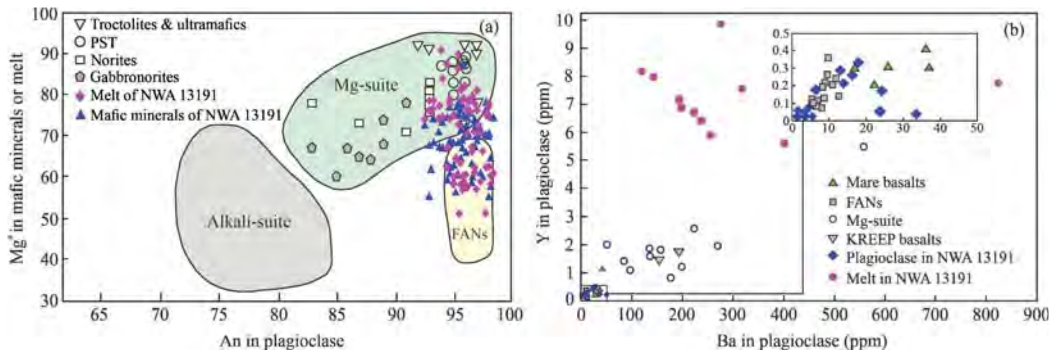

Always consult and cite the final, published document. See http:/www.minsocam.org or GeoscienceWorld